CleanMat

WILEY

CleanMat

REVIEW OPEN ACCESS

Biochar Adsorption: A Green Approach to PFAS Contaminant Removal

Darshana Chavan[1] | Neelaambhigai Mayilswamy[2] | Satkirti Chame[3] | Balasubramanian Kandasubramanian[2]

[1]Department of Microbiology, Sinhagad College of Science, Pune, India | [2]Nano Surface Texturing Lab, Department of Metallurgical and Materials Engineering, Defence Institute of Advanced Technology (DU), Pune, India | [3]Department of Chemical Technology, Institute of Chemical Technology (ICT), Jalna, India

Correspondence: Balasubramanian Kandasubramanian (meetkbs@gmail.com)

Received: 13 June 2024 | **Revised:** 5 December 2024 | **Accepted:** 6 December 2024

Funding: The authors received no specific funding for this work.

Keywords: adsorption kinetics | biochar | isotherms | machine learning | PFAS toxicity assessment

ABSTRACT

The widespread use of PFAS in nonstick cookware, hydrophobic textiles, stain-resistant fabrics, cosmetics, and floor coverings has led to their persistent presence in wastewater streams, posing significant human health and ecological risks. Exposure to PFAS is linked to adverse reproductive outcomes and elevated blood pressure in pregnant individuals, and it negatively impacts aquatic ecosystems, particularly algal populations and microbial communities. This evaluation focuses on biochar's efficacy and cost-efficiency in removing PFAS from water, highlighting its potential as a sustainable remediation method. Biochar's high microporous volumes (0.1–1.0 cm^3/g), aromaticity, and surface oxygen-containing functional groups make it effective for PFAS adsorption. Various biochar production methods, such as pyrolysis of biomass waste, and innovative modification techniques like acid treatment, ball milling, and metal nanoparticle incorporation are explored to enhance PFAS adsorption capacity. The mechanisms, kinetics, and thermodynamics of PFAS adsorption onto biochar are examined, providing insights into molecular-level interactions and adsorption isotherms. Furthermore, machine learning models are utilized to understand the impact of processing parameters on PFAS removal efficiency. The review also presents toxicological studies on the harmful effects of PFAS exposure on organisms and humans, emphasizing the urgent need for effective remediation strategies. Ultimately, the potential of biochar-based approaches in treating PFAS-contaminated water is underscored by optimizing its physicochemical properties through innovative production and modification methods, along with predictive modeling of adsorption behavior.

1 | Introduction

PFAS, or Per- and polyfluoroalkyl substances, constitute a category of artificial compounds extensively employed across consumer and industrial sectors since the 1940s owing to their favorable characteristics, including resistance to staining and water repellency [1]. However, the carbon-fluorine bonds that give PFAS these properties also make them impervious to degradation and extremely insistent in the environment [2]. This has raised significant concerns about their potential for bioaccumulation and antithetical ramifications on ecological systems and anthropogenic well-being. In 2016, the United States Environmental Protection Agency (EPA) delineated health advisory benchmarks at 70.0 parts per trillion (ppt) or 0.07 μg per liter (μg L^{-1}) for perfluorooctanoic acid (PFOA) and perfluorooctane sulfonate (PFOS) in drinking water, aiming to offer Americans, particularly vulnerable groups, a safeguard against potential long-term exposure to these

substances. A drawback associated with PFAS usage is their entry into the water cycle, either via direct routes like runoff and infiltration into groundwater from nonpoint sources, or through specific sources like firefighting training areas, industrial sites, and discharge from wastewater treatment plants —both municipal and industrial—or even through deposition from the atmosphere [3]. A growing body of epidemiological evidence links PFAS exposure to a variety of adverse health outcomes in humans, including impacts on vital organs like the liver, kidneys, immune system, and thyroid [4, 5]. PFAS have also been shown to exhibit bioaccumulative behavior within the environment, posing risks to wildlife across aquatic and terrestrial food webs [4, 6]. Their ubiquitous presence, even in remote areas, underscores their remarkable persistence and mobility [2, 4].

In light of these concerns, effective remediation approaches are crucial to address PFAS contamination in water sources. The review discusses the hazard index, a tool the EPA (Environmental Protection Agency) uses to evaluate health risks associated with chemical mixtures containing PFAS compounds. It takes into account the different toxicities of specific PFAS (Per- and polyfluoroalkyl substances) like PFNA (Perfluorononanoic acid), GenX chemicals, PFHxS (Perfluorohexane sulfonate), and PFBS (Perfluorobutane sulfonate) to determine if their joint levels in drinking water systems are alarming. Also explores the potential of biochar, a carbonaceous substance derived from the pyrolytic decomposition of biomass, as an efficacious adsorbent for the removal of per- and polyfluoroalkyl substances (PFAS) from aqueous solutions [7–9]. It also delves into the toxicological impacts of PFAS, their mechanisms of entry into the environment, and the adsorption processes involved in using biochar for their removal [10–12]. It highlights the importance of tailoring biochar's chemical and physical properties through careful selection of feedstock materials, pyrolysis conditions, hydrothermal carbonization, gasification, torrefaction, flash carbonization process, and modification techniques to enhance its PFAS adsorption efficiency [13, 14]. It also provides insights into the underlying adsorption mechanisms, kinetics, and thermodynamics [15, 16]. Furthermore, confers the potential of machine learning approaches, for example, tree-based methods and neural networks, for accurately predicting PFAS removal rates based on various process factors like adsorbent characteristics and equilibrium concentrations [17]. Overall, this review serves as a treasured resource for understanding the challenges posed by PFAS contamination and the potential of biochar-based solutions, coupled with machine learning models, for sustainable and scalable treatment of PFAS-contaminated water [18, 19].

2 | PFAS and Its Toxicity

PFAS, denoting perfluoroalkylated and polyfluoroalkylated substances, encompass a spectrum of artificial compounds distinguished by a hydrophobic alkyl chain of varying lengths, commonly comprising between 4 and 16 carbon atoms. These chains can be partially fluorinated or fully fluorinated, meaning some or all of the hydrogen atoms are replaced by fluorine atoms, respectively. Additionally, PFAS contains a hydrophilic group [20]. When the alkyl chain undergoes partial fluorination, these compounds are denoted as polyfluoroalkyl substances, while those with fully fluorinated chains, except for specific hydrogen atoms that may be part of functional groups, are known as perfluoroalkyl substances. Polyfluoroalkyl substances can probably convert into perfluoroalkyl substances through environmental degradation processes [21]. Figure 1 describes two main categories: 1. Non-polymeric perfluoroalkylated substances, which consist of - Perfluoroalkylated acids (PFAA), are further divided into subcategories such as perfluoroalkane sulfonic acids (PFSA) and per-fluoroalkyl carboxylic acids (PFCAs). (a) phosphinic acids (PFPIAs) and Perfluoroalkyl phosphonic (PFPAs). (b) Perfluoroalkane sulfonamide (PFASAs). (c) Perfluoroalkyl iodide (PFAIs). 2. Non-polymeric polyfluoroalkylated substances, which include: (a) Perfluoroalkane sulfonamides. (b) Fluorotelomer substances, subdivided into fluorotelomer alcohols (FTOH) and polyfluoroalkyl phosphoric acid esters, fluorotelomer phosphates (PAP), and polyfluoroalkyl phosphates. The image provides a detailed breakdown of each category and subcategory, along with examples of specific compounds.

The potential deleterious health ramifications of PFAS may exhibit significant variability contingent upon parameters such

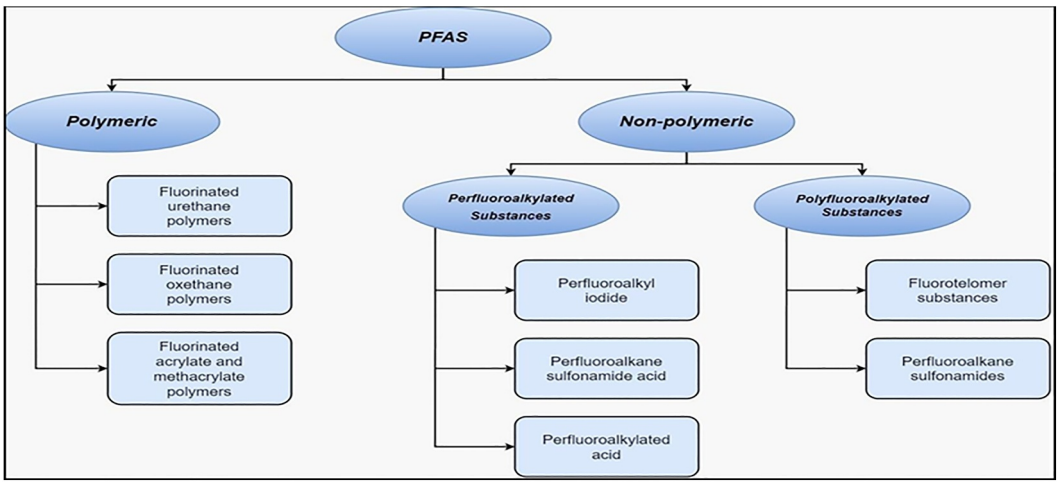

FIGURE 1 | Categorization of per-fluoroalkylated and polyfluoroalkylated compounds.

as the magnitude, duration, and modality of exposure, alongside individual attributes encompassing age, sex, ethnicity, overall physiological state, and genetic predisposition [22]. Based on contemporary scientific understandings, the multifaceted toxicological effects of PFOAs are notably due to nuclear receptor activation, the induction of oxidative stress, or the direct trepidation of cellular membranes [23]. Even at the diminished concentrations, there exists the potential for the onset of thyroid dysfunctions, and adverse repercussions on fertility rates, embryonic development, or impairments of motor functions. In aquatic organisms such as zebrafish, the change in steroid levels was observed at a concentration of 10^{-5} g/L. The toxic effects on insect larvae such as dragonflies or chironomids are being affected at a concentration range of (2–10) $\times$ 10^{-5} g/L. Africa clawed frogs exhibited hepatic cellular degeneration; moreover, at a mere 0.1 μg L^{-1} concentration of PFOS, there was an upregulation in the expression of TRbA mRNA within the cerebral and caudal tissues, serving as a sensitive indicator for thyroid dysfunction. The growth of invertebrates, including reptiles like Bahama Anolis, is notably diminished when exposed to low concentrations of PFOS.

Figure 2 depicts the certainty levels concerning the presence of PFAS within the human body and the organs they affect. The dotted lines represent areas of low certainty, indicating uncertainty regarding PFAS presence or their impact on specific organs. In contrast, the straight lines signify high certainty, suggesting a well-established understanding of PFAS distribution and their effects on particular organs. Once ingested the PFAS are absorbed into the bloodstream and distributed throughout the body, where they exhibit a propensity to bioaccumulate in protein-dense tissues, notably the hepatic and renal systems [25]. It also tends to affect the thyroid, immune system, and the embryo inside the pregnant woman. The liver especially susceptible, with PFAS exposure correlated with modifications in hepatic enzyme levels and potential hepatotoxicity [26]. The renal system is similarly compromised, as PFAS can impair renal function and elevate the risk of chronic nephropathy [27]. Furthermore, PFAS can interfere with thyroid dysfunction. The immune system is another pivotal target, with research indicating that PFAS exposure can attenuate antibody production and heighten vulnerability to infections. Endocrine disruptions in pregnant women have been documented even at relatively low concentrations of PFAS, particularly those with long-chain structures. These compounds notably perturb thyroid hormone levels and sex hormone balance, leading to profound and enduring ramifications [28]. In a developing fetus, PFAS can cross through the placenta, leading to in-utero exposure which is associated with detrimental gestational outcomes, including pre-eclampsia and reduced neonatal birth weight. In the developing fetus, this hormonal imbalance can adversely affect the maturation of critical organs such as the genitals, liver, kidneys, and brain. For the mother, such disruptions are linked to metabolic disorders, including gestational diabetes, underscoring the extensive impact of PFAS on both maternal and fetal health [26].

Per-fluoroalkyl and poly-fluoroalkyl substances (PFAS), encompassing over 4700 synthetic chemicals, have had widespread industrial and consumer applications since the 1940s due to their desirable properties like stain repellency and water resistance. However, these properties, conferred by robust carbon-fluorine bonds, raise concerns regarding their potential for environmental persistence, bioaccumulation, and toxicological effects. A growing body of epidemiological evidence links PFAS exposure elicits a spectrum of detrimental health outcomes in humans, impacting crucial organs, including the

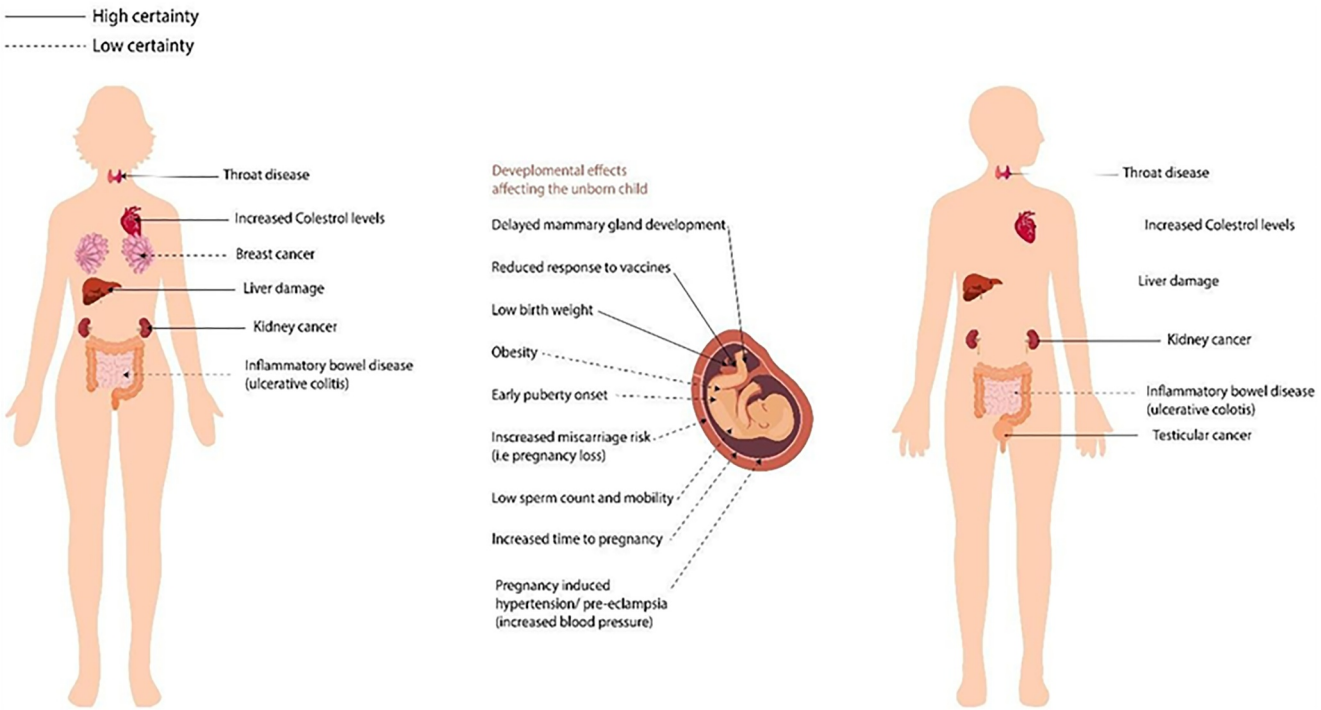

FIGURE 2 | Certainty of PFAS in the human body and organs it affects. Reprinted with permission from [24]. Copyright 2020, Wiley.

hepatic systems, renal systems, immune apparatus, and thyroid gland [29]. Early-life exposure is particularly worrisome as PFAS can readily traverse the placenta and accumulate in breast milk. Studies have established correlations between PFAS exposure and elevated cholesterol levels, compromised hepatic function, diminished immune response, thyroid dysfunction, reduced fertility, developmental anomalies, and even an increased risk of cancers [4] The threat extends beyond human health, as PFAS exhibit bio accumulative behavior within the environment, posing a significant risk to wildlife across aquatic and terrestrial food webs [30, 31]. Scientific investigations have documented a variety of adverse effects in exposed animals, including hepatic damage, thyroid disorders, immunotoxicity, reproductive and developmental impairments, neurotoxicity, and tumor formation [30, 31]. The ubiquitous presence of PFAS, even in remote areas, underscores their remarkable persistence and mobility [2, 4]. Aquatic organisms are particularly susceptible, with documented cases of developmental delays, fin erosion, and mortality in fish populations PFAS exposure in avian species has been linked to diminished hatching success and hormonal disruptions, potentially contributing to population-level declines observed in sea otters, for instance [4]. While the intricate effects of PFAS mixtures on ecosystems require further elucidation, studies have demonstrated their toxicity toward various algal and microbial communities. This disrupts algal growth and reproduction, potentially cascading negative effects throughout the food web [2].

Figure 3 shows a few significant indirect ways that exposure to PFAS may affect neurological health by impairing the activities of the kidney, liver, and peripheral immune system. Toxic drug accumulation and inflammatory molecule buildup in the bloodstream can harm neurons, impair the blood-brain barrier, and exacerbate neurodegenerative disorders. Additionally, PFAS are PPAR agonists, and as PPARs are abundant in the brain, liver, kidneys, and immune system, they provide a significant molecular target for the direct and indirect impact of PFAS on neurological health [32].

Risk assessments play a crucial role in defining public health exposure thresholds, which in turn establish requirements for exposure mitigation tactics and ecological remediation initiatives. Table 1 conducts a comprehensive analysis of the impacts of PFAS on the environment and various organisms.

Considering the adverse ecological consequences of PFAS and PFOS on the environment and their persistence in water systems research has been conducted to remediate this problem and a multitude of materials have been employed in this field. Therefore, the maximum permissible concentration of perfluorooctanoic acid is 100 ng L^{-1}. The temporal resolution for detecting PFAS in wastewater could be exceptionally rapid, frequently within 10 min, utilizing sophisticated methodologies such as time-series data analysis and microfluidics-based sensors. These advanced techniques facilitate the expeditious

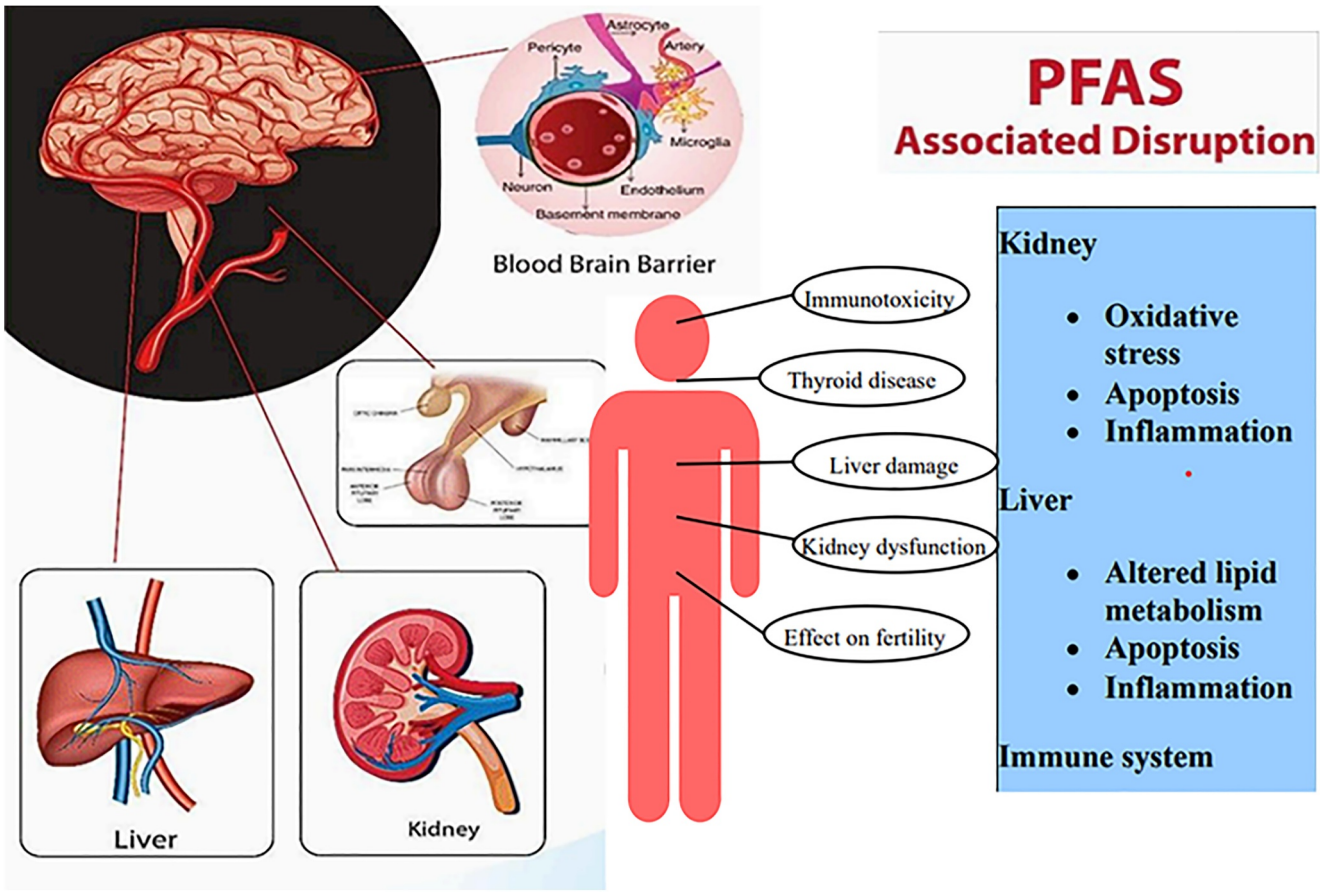

FIGURE 3 | PFAS associated disruption.

TABLE 1 | Effect of PFAS on various organisms in the ecosystem.

Sr. No.	Organism (common Name)	Organism (scientific name)	PFAS type	Toxic effects	References
1	Green mussel	Perna viridis	PFOS, PFOA, PFNA, and PFDA	DNA damage, oxidative damage, membrane instability, and reduced body weight	[33]
2	Pearl mussel	Hyriopsis cumingii	PFOS	Oxidative stress, cellular detoxification	[34]
3	Chinese mitten crabs	Eriocheir sinensis	PFOS	Affects gill respiratory metabolic enzyme cytochrome C oxidase and hemolymph hemocyanin content.	[35]
4	Sea urchin	Glyptocidaris crenularis	PFOS	Decrease in red blood cells, transient diminution of movement, increased methylation levels	[36]
5	Red worm	Limnodrilus hoffmeisteri	PFOS	Changes on GSH levels, MDA content and SOD activity	[37]
6	Typical water flea	Daphnia magna	PFOS	Increased heart rate, inhibitory effects on breeding rates.	[38]
7	Freshwater rotifer	Brachionus calyciflorus	PFOS	Juvenile period, affecting body size, net reproductive rate, and smaller egg size.	[39]
8	Green algae	Tetradesmus obliquus	PFOA, PFDOA, PFTEA, PFOS	Inhibited proliferation rate, decrease in chlorophyll content	[40, 41]
9	Microalgae	Pseudokirchneriella subcaptitata	PFOS, PFOA, PFBS, and APFO	Reduced growth rate after prolonged exposure	[37]
10	Chlorella	Chlorella vulgaris	PFOS	Concentration-dependent ROS elevation, augmented malondialdehyde (MDA) levels, alterations in chlorophyll concentration and chloroplast morphology, and oxidative injury	[42]
11	Marine bacterium	Vibrio fischeri	PFOS and PF-656	Luminescence inhibition.	[43]
12	Purple sea urchin	Strongylocentrotus purpuratus	PFOS and PFOA	Highly toxic	[44]
13	Water flea	Daphnia carinata	PFOS	Damaged genetic makeup, high mortality, and elevated birth defects	[45]
14	American bullfrog	Rana catesbeiana	PFOS and PFOA	Variation in snout-vent length	[46]

classification and quantification of PFAS by analyzing their distinct chemical signatures [47].

Figure 4a illustrates the concentrations of the presence of perfluorooctanoic acid (PFOA) and per-fluorooctane sulfonate (PFOS) in potable water sources and distribution systems worldwide, with notably elevated levels observed in the United States (US) and Sweden. In the US, both drinking water sources and supplies exhibited maximum PFOA concentrations of 11,000 ng L^{-1} and 4300 ng L^{-1}, respectively, In Swedish drinking water sources, the most elevated levels of PFOS were detected, with concentrations reaching 2280 ng L^{-1}, while in distribution systems, they peaked at 8000 ng L^{-1}. These nations, well-known for their substantial per- and poly-fluoroalkyl substances (PFAS) manufacturing and utilization activities, represent significant contamination hotspots. Despite the cessation of PFAS production in initial manufacturing nations, there has been a discernible surge in manufacturing within developing regions. In Ghana, tap water obtained from River Kakum and River Pr supplied to nearby communities exhibited relatively elevated concentrations of perfluorooctanoic acid (PFOA: 190.0 ng L^{-1}) and PFOS (168.30 ng L^{-1}). Brazil likewise documented PFAS acquaintance through tap water (PFOA: 46.0 ng L^{-1}; PFOS: 44.0 ng L^{-1}) and bottled water (PFOA: 12.0 ng L^{-1}), with variations noted among bottled water samples from distinct marketplaces. Korean tap water specimens displayed notably higher mean PFOA concentrations (12.87 ng L^{-1}) compared to bottled water samples (0.16 ng L^{-1}), suggesting the potential presence of PFAS in the primary potable water reservoir, specifically surface water, signifies a significant concern within the domain of environmental and public health. Analogously, Hong Kong's water distribution exhibited elevated PFOA levels in tap water (39.7 ng L^{-1}) and bottled water (32.6 ng L^{-1}), followed by PFOS. Remarkably, bottled water in Thailand demonstrated higher PFAS levels compared to tap water, indicating a potential influence of bottled materials on water quality. Furthermore, the graphical representations in Figure 4b,c elucidate the proportional concentrations of per-fluorooctanoic acid (PFOA) and per-fluoro octane sulfonate (PFOS) global potable water sources and

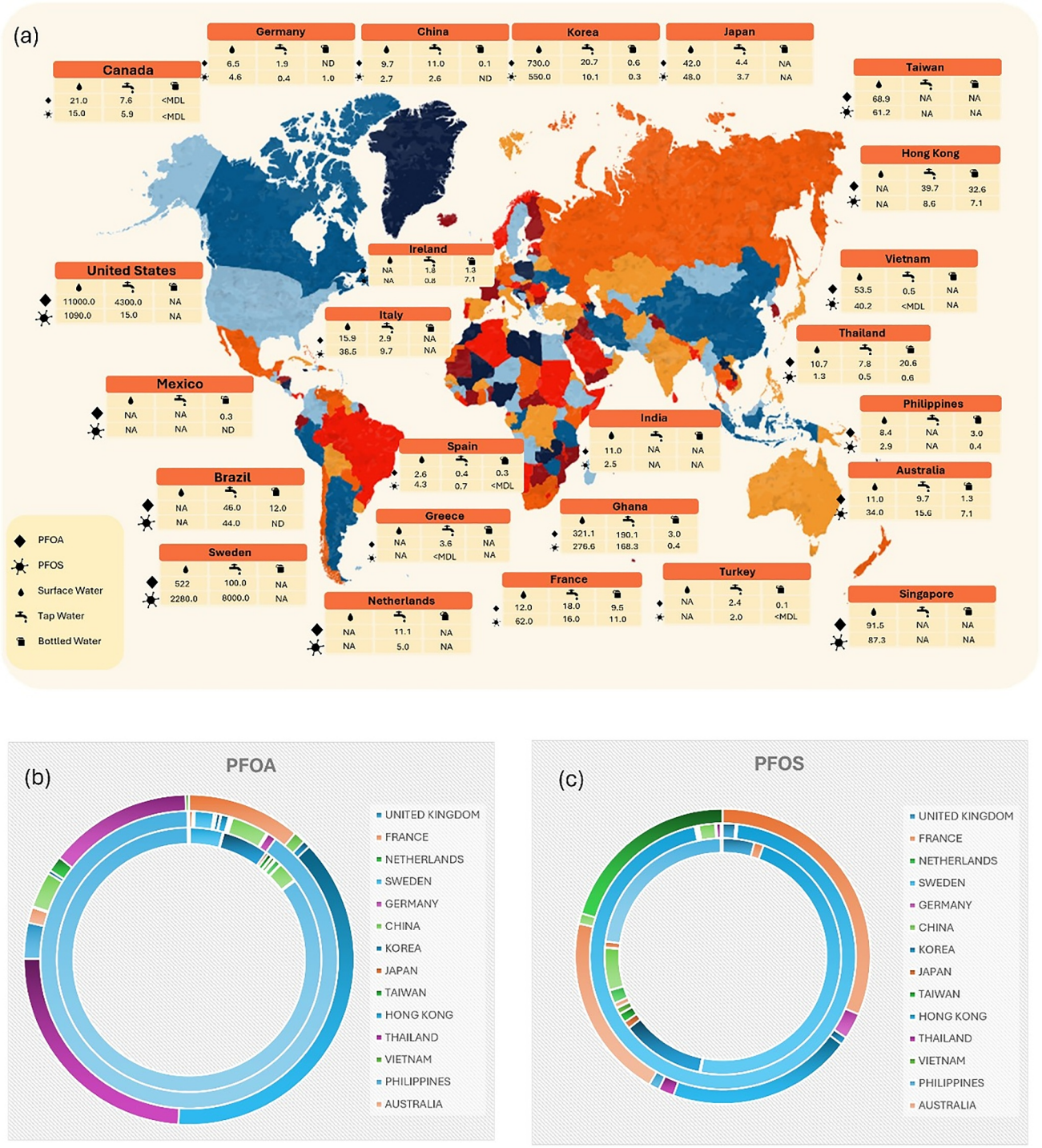

FIGURE 4 | (a) Illustrates the concentrations of per-fluorooctanoic acid (PFOA) and perfluoro octane sulfonate (PFOS) in worldwide potable water sources and distribution systems, (b) depicts the percentage levels of PFOA, and (c) Illustrates the proportions of PFOS present in drinking water sources and distributions worldwide. Reprinted with permission from [48]. Copyright 2023, Nature.

distribution networks, unveiling analogous pollution levels across diverse regions worldwide [30–58].

3 | Hazard Index

The Hazard index is a longstanding instrument employed by the EPA to assess the health risks posed by chemical mixtures, such as in the Superfund program. A Hazard Index MCL is being proposed by the EPA to limit any mixture that includes one or more of PFHxS, PFNA, PFBS, and/or GenX Chemicals. The Hazard Index takes into account the different toxicities of PFNA, GenX Chemicals, PFHxS, and PFBS. Water systems would practice the use of hazard index calculation for these PFAS to determine whether the total quantity of these PFAS in the drinking water in the system is alarming and requires action.

Enumeration of the Hazard Index:

The Hazard Index is composed of a total of fractions (HI). Each percentage compares the maximum amount of PFAS that has been shown to be safe for human health to the amount of PFAS present in the water. Equation (1) represents the following.

Equation:

$$\text{Hazard Index (HI)} = \left(\frac{[\text{GenX water}]}{[10\ \text{ppt}]}\right) + \left(\frac{[\text{PFBS water}]}{[2000\ \text{ppt}]}\right) + \left(\frac{[\text{PFNA water}]}{[10\ \text{ppt}]}\right) + \left(\frac{[\text{PFHxS water}]}{[9.0\ \text{ppt}]}\right) \quad (1)$$

Stage I: Divide the measured Gen X concentration by the 10 ppt health-based threshold.

Stage II: Divide the PFBS concentration that was measured by the 2000 ppt health-based threshold.

Stage III: Divide the PFNA concentration that was measured by the 10 ppt health-based value.

Stage IV: Divide the recorded PFHxS concentration by the 9 ppt health-based threshold.

Stage V: Combine these ratios acquired in Stage I with those from Stage IV.

Stage VI: Repeat steps 1 through 5 for each sample obtained during the previous year to determine HI compliance. Next, calculate the mean HI for all samples collected during the preceding year.

Stage VII: If the ongoing yearly average HI surpasses 1.0, it constitutes a breach of the suggested HIMCL

4 | Chemical Mechanisms for PFAS Destruction

PFAS (Per-fluoroalkyl and poly-fluoroalkyl) substances are a Category of synthetic chemicals known for their environmental persistence due to their strong C-F (carbon-fluorine bonds). Their occurrence in water is a growing alarm due to their probable health risks. Although thermal treatment, landfill disposal, and underground injection are employed for PFAS management, thermal treatment provides a certain level of destruction.

4.1 | Defluorination

Defluorination is a well-established linkage for initiating the degradation of per and PFAS (polyfluoroalkyl substances) during remediation. It typically serves as the first step in various treatment technologies, including reduction, photocatalysis, hydro defluorination, and HALT (hydrothermal alkaline treatment), microbial metabolism. These processes can be categorized by the type of defluorination employed: reductive (electron transfer) or nucleophilic replacement (hydroxide ion). The location of defluorination within the PFAS molecule is influenced by the inherent weakness of specific carbon-fluorine (C-F) bonds and the distribution of the smallest lying σ*C-F orbitals. However, the overall degradation pathway and products are significantly affected by reaction situations, such as temperature, solvent, and the occurrence of other reactive species. Following defluorination, a cascade of secondary reactions can ensue, including hydrogen abstraction, further electron transfer and defluorination, and radical addition. These secondary reactions can lead to a diverse array of products, including perfluoroalkyl radicals, perfluoroalkenes, shortened perfluoroalkyl chains (PFCAs), and a complex mixture of fluorinated compounds from radical recombination. Notably, hydrodefluorination using silylium-carborane catalysts represents a new and promising technique for PFAS degradation, but further research is required to validate its efficacy across a wider range of PFAS contaminants.

4.2 | Ablation of the Polar Head Moiety

Beyond defluorination, the elimination of the polar head group (carboxylate for PFOA and sulfonate for PFOS) is another key mechanism for PFAS degradation. This mechanism is observed in oxidation (e.g., activated persulfate), photocatalysis, plasma treatment, and potentially other techniques. Oxidation with strong oxidants like sulfate radicals creates a perfluoroalkyl radical intermediate. For PFCAs, this intermediate undergoes a cyclic decarboxylation-hydroxylation-elimination-hydrolysis (DHEH) process, leading to the gradual shortening of the perfluoroalkyl chain. While a similar mechanism hasn't been confirmed for PFOS desulfonation, plasma treatment cleaves the sulfonate group and potentially utilizes the DHEH mechanism for chain shortening. Plasma treatment likely involves both head group removal and defluorination via electron transfer. Recent research suggests argon cations in plasma promote head group oxidation while aqueous electrons contribute to defluorination. Interestingly, studies report PFAS degradation in polar aprotic solvents with sodium hydroxide, potentially via a decarboxylation mechanism forming a perfluorinated carbanion. This carbanion undergoes a proposed three-carbon chain shortening (C3) mechanism, but the requirement for non-aqueous solvents limits its real-world applicability.

4.3 | Unimolecular Bond Scission and Other Initialization Mechanisms

Thermal decomposition and sonolysis are two key mechanisms for PFAS destruction. The high bond strength in PFAS (> 85 kcal mol^{-1} for C-C and > 100 kcal mol^{-1} for C-F) makes unimolecular bond scission unlikely at typical temperatures. Thermal decomposition, dominating at high temperatures, involves a series of reactions. Initially, PFCAs and PFSAs undergo HF elimination to form unstable intermediates (α-sultone and α-lactone correspondingly). These intermediates then react further to form perfluoroacyl fluoride products. At even higher temperatures, H-shift and removal of CO_2 and HF lead to the

creation of perfluoro-1-alkenes. All these products can further degrade into volatile fluoro organic compounds. Sonolysis, on the other hand, utilizes high localized temperatures generated during bubble rupture in ultrasound treatment. This extreme heat is believed to cause cleavage of the polar head group (C-S or C-C bond) through unimolecular scission. The mechanism likely proceeds via repetitive oxidation and truncation or pyrolysis inside the bubble. However, the variability in temperature, presence of reactive intermediates, and the type of PFAS undergoing degradation leads to a complex overall mechanism and a mixture of products.

Conventional methods for PFAS remediation, like landfill disposal, underground injection, and thermal treatment have significant drawbacks. While thermal treatment offers some destruction, it requires high energy and can generate harmful byproducts. Landfills and injections simply concentrate PFAS, posing future contamination risks if liners fail [49]. Biochar emerges as a potentially superior alternative due to its ability to both adsorb and potentially degrade PFAS molecules. This offers a more sustainable destruction pathway compared to mere concentration. Additionally, biochar is produced from organic waste materials, promoting waste diversion and carbon sequestration. Furthermore, its production from readily available materials makes it cost-effective compared to high-energy thermal treatment [50].

5 | Biochar and Production Techniques of Biochar

Biochar is a carbon-rich material generated from the thermolytic degradation of organic biomass in Anaerobic conditions and has garnered noteworthy consideration in current years due to its diverse applications and likely benefits. The utilization of biochar for diverse applications has spurred heightened modification of biomass into biochar. Biochar is favored over alternative adsorbents due to its economic viability, exceptional adsorption efficacy, and environmentally benign characteristics. Also, one of the advantages of utilizing biochar is that it could be tailored according to the contaminant sequestration [51, 52]. Thermochemical conversion serves as a prevalent method for biochar production, encompassing techniques like pyrolysis, gasification, hydrothermal carbonization, and torrefaction. Synthesized from biomass via pyrolysis, biochar exhibits an elevated specific surface area, intricate porous architecture, and a plethora of functional groups, rendering it exceptionally proficient in the adsorption of a diverse array of pollutants [53]. To achieve extreme biochar yield, the selection of the production technique must be tailored to the biomass nature, and optimal process settings such as heating rate, residence time, and temperature are essential. These conditions are critical as they can impact biochar's chemical and physical properties throughout production [54]. The properties of biochar can be varied according to the feedstock and the modifications done on the surface of the biochar by inducing chemical and physical modifications. These biochar capabilities have attracted a lot of attention in the field of wastewater treatment. To generate biochar, thermochemical methods such as pyrolysis, hydrothermal carbonization, gasification, torrefaction, and flash carbonization are routinely utilized [55, 56]. In pyrolysis, the factors determining the biochar production depend on the temperature and the type of biomass used. Usually, the temperature range is 200°C–950ºC. The waste biomass is converted into value-added products such as biochar, biogas, and bio-oil. The mechanism of the pyrolysis is represented in Figure 5a [57]. Figure 5b represents the low-temperature circulating fluidized bed gasifier that utilizes high contents of low-melting ash compounds. The temperature of such a reactor is kept below the melting point of the ash components to avoid corrosion [58]. In hydrothermal carbonization, the temperature range is kept low around 150°C–300ºC, and the product is referred to as Hydrochar. The biomass is mixed along with water and placed in a closed reactor. The different types of products produced during this process include biochar, bio-oil, and syngas (Figure 5c) [57]. Torrefaction is a method that is conducted in oxygen oxygen-deprived environment with a lagging heating rate. This method is carried out in 4 steps: heating, dehydrating, torrefy, and condensing (Figure 5d) [59]. Figure 5 illustrates various methods for producing biochar, including pyrolysis (a), gasification (b), hydrothermal carbonization (c), and torrefaction (d).

Table 2 below describes the different categorization techniques of biochar Chemical, Physical, and stability of Biochar. The table summarizes key physical and chemical properties of biochar compositions. It includes measurements such as elemental analysis (CHNS, EDS, XPS), and metal/ash content determination (XRD, ICP, XRF). Proximate analysis via TGA reveals hydrous content, volatile constituents, and ash residue. Surface functionality is assessed using FTIR and Raman spectroscopy, while Boehm titration is used to measure surface acidity/alkalinity. Surface aromaticity is analyzed via Raman spectroscopy and 13C NMR. Physical properties include surface area, size, pore volume, density measurements, pycnometer, and laser sizing for particle size distribution. Lastly, stability is evaluated with TGA-DSC and thermogravimetric analysis, shedding light on thermal properties and degradation behavior. A detailed analysis of biochar's characterization is provided below in Table 2.

6 | Biochar Modification Techniques

Engineered biochar shows an enhanced contamination sorption through an enhanced sorption mechanism to vanquish this lack of pristine biochar, synthesizing composites is envisioned to improve electrostatic attraction between anionic (PFAS) [2]. Biochar can be modified using various techniques to meet the demands of certain applications. Biochar undergoes discernible alterations at both physical and chemical levels. Physical modifications encompass changes in surface morphology, pore structure, and specific surface area, while chemical modifications involve alterations in functional groups, elemental composition, and surface reactivity, while physical modifications include ball milling. Excellent performance can be obtained via chemical techniques, which require a low activation temperature and are upfront to accomplish. Physical and chemical modifications of biochar play a pivotal role in augmenting its properties for diverse applications. Through techniques such as activation and pyrolysis temperature control, biochar's porosity can be finely tuned, leading to increased surface area and enhanced adsorption

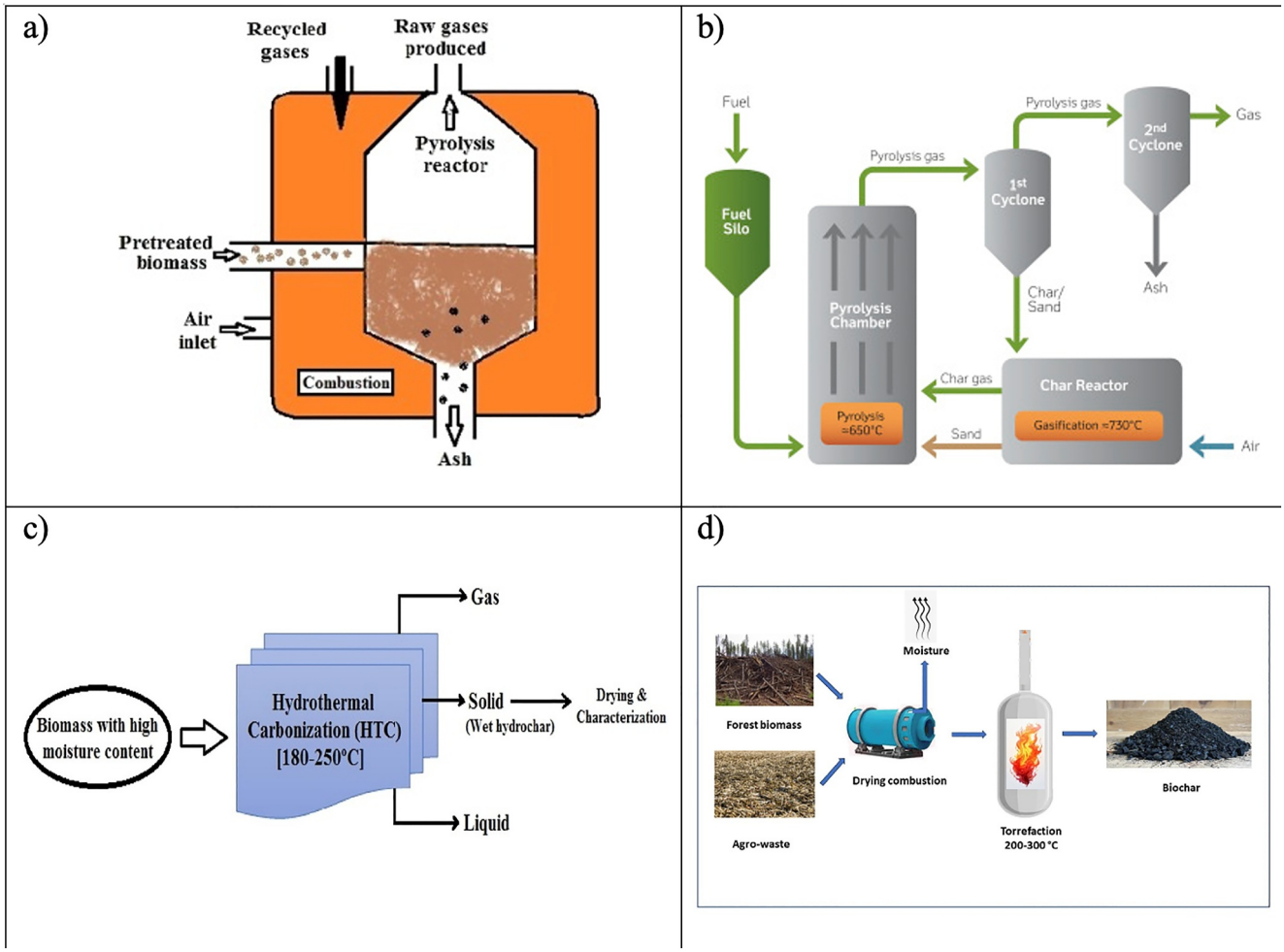

FIGURE 5 | Schematic representation of (a) Pyrolysis. Reprinted with permission from [57]. Copyright 2020, Elsevier; (b) Gasification. Reprinted with permission from [58]. Copyright 2015, Elsevier; (c) Hydrothermal Carbonization. Reprinted with permission from [57]. Copyright 2020, Elsevier; and (d) Torrefaction. Reprinted with permission from [59]. Copyright 2024, Springer.

TABLE 2 | An in-depth overview of the characterization of biochar.

Characterization	Detailed analysis
Chemical property	• Biochar compositions (CHNS, XPS, EDS)
	• Metallic/ash contents (XRD, XRF, ICP) proximate analysis (TGA)
	• Surface functionality (Raman, FTIR)
	• Boehmtitration surface, aromaticity, surface, acidity/alkalinity (Raman spectroscopy, 13C NMR)
Physical property	• Surface area and pore volume
	• Particle size distribution (lasersizing)
	• Density (mercury porosity, pycnometer)
Stability	TGA-DSC DSC (differential scanning calorimetry) and TGA (thermogravimetric analysis)

capacity for contaminants and nutrients. Also, this mechanical treatment of ball milling breaks down the biochar particles into finer sizes, enhancing their surface reactivity and interaction with contaminants by the modification of surface functional groups. Additionally, chemical treatments such as impregnation with alkali or acids can introduce functional groups (hydroxyl, carboxyl, amino groups) onto the biochar surface that in turn increases the biochar's affinity toward PFAS through

mechanisms such as hydrogen bonding, electrostatic interactions, and ion exchange, improving its reactivity and adsorption properties. For instance, acid modification results in incorporation of oxygen-bearing functional moieties enhancing cation exchange capacity. While alkali on the other side increases the aromaticity and hydrophobicity of biochar improving its ability to adsorb contaminants through π-π interactions [60]. These modifications not only boost biochar's ability to adsorb various contaminants, including heavy metals and organic pollutants but also enhance its capacity to retain essential nutrients like nitrogen and phosphorus, fostering soil fertility and plant growth. Moreover, modified biochar exhibits increased stability, prolonging its effectiveness as a sustainable soil amendment and environmental remediation tool [61].

Figure 6 shows Innovative approaches such as internally modified pyrolysis and steam modification methodologies are employed to augment biochar's surface area and sorption characteristics. Ball milling techniques yield substantial enhancements in pollutant adsorption efficacy by mechanically reducing the particle size of biochar. It can enhance the precise surface area of biochar to a range of 200–400 $m^2 g^{-1}$ [62]. At the same time, acid and alkali modifications elicit alterations in surface chemistry and pore morphology, respectively, thereby ameliorating the environmental remediation potential of biochar materials. Acid treatments with agents such as HCl or HNO_3 introduce a substantial quantity of oxygen-bearing functional groups including, carboxyl and hydroxyl moieties, thereby augmenting the cation exchange capacity and adsorption efficacy for organic pollutants. Conversely, alkaline modifications employing substances like KOH or NaOH bolster π-π interactions between the adsorbate and the pollutants, further improving adsorption performance [60].

Table 3 outlines various modifications of biochar, detailing their associated processing parameters and specific surface area values. Each entry includes a type of biomass used, the specific modification applied, the effects of the modification, relevant processing parameters, specific surface area values achieved, and corresponding references for further information.

7 | Remediation of PFAS Containing Wastewater Using Biochar-Based Adsorption

Since the beginning adsorption has emerged as a vital process for pollutant removal across various scientific disciplines due to its effectiveness and relative simplicity [66]. Biochar, a carbonaceous material produced from biomass pyrolysis, has garnered significant attention as a promising adsorbent for its high microporous volume, surface aromaticity, and cost-effectiveness [67]. Employing a modified biochar for the abatement of PFAS is highly efficacious owing to its superior adsorption capacity and the presence of diverse functional moieties that facilitate the cleavage of the resilient C-F bonds inherent in PFAS compounds. A recent study by Krebsbach et al. (2023) explored optimizing biochar design for enhanced removal of per- and polyfluoroalkyl compounds (PFAS) from water [68] Their research suggests that pore size plays a critical role in PFAS adsorption, with biochars exhibiting smaller pores and produced at higher pyrolysis temperatures demonstrating superior removal efficiency. Furthermore, research conducted by Patel et al. investigating the use of biochar derived from biosolids for both anaerobic digestions, a process generating biogas from wastewater, and subsequent PFAS removal [61]. This approach presents a sustainable wastewater treatment strategy by combining resource recovery through biogas production with pollutant capture. Moving forward, further research is necessary to validate biochar's effectiveness in real-world environmental settings and refine its composition for widespread PFAS remediation efforts [68].

Table 4 below provides a condensed overview of numerous studies focusing on the adsorption of per- and polyfluoroalkyl compounds from water using biochar. Each entry in the table delineates critical information, including the type of biomass

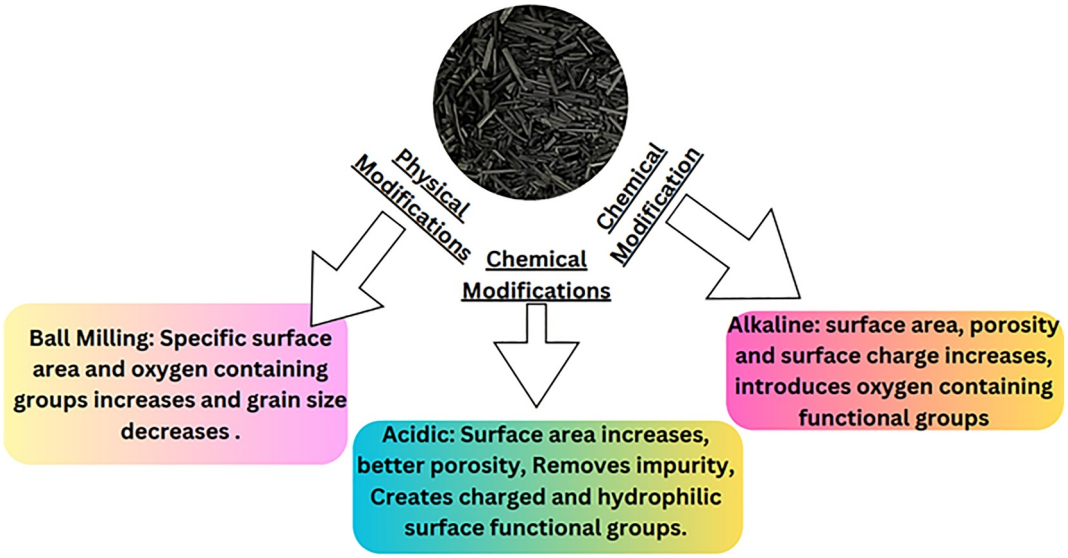

FIGURE 6 | Description: Enhancing biochar properties through modifications.

TABLE 3 | Biochar modifications encompassing their processing parameters and specific surface area values.

Sr. no.	Biomass type	Modification	Effects of modification	Processing parameter	Specificsurface area (m^2/g)	References
1	SCG (spent coffee grounds)	Chemical modification- activated by alkaline hydroxide	Increased efficiency of coffee grounds eliminated: ~10%–99% of PFOS	Carbonization at 2000°C at 100°C/min for 1h pH = 3 Max. Adsorption capacity = 43.40 mg/g Biochar dose = 100 mg L^{-1} Adsorbent dose = 5 mg Equilibrium time = 24 h.	—	[63]
2	Douglas fir biochar	Chemical modification- treated with $FeCl_3/FeSO_4$ and NaOH to chemically precipitate Fe_3O_4	Magnetic Fe_3O_4 sorption was quick (15–40 min). Quantity: (a) PFOA ~653 mg/g (b) PFOS ~14.5 mg/g	Gasification temperature: 900°–1000°C for 1–20 s pH = 6–8 Equilibrium time = 20–45 min.	700 m^2/g	[2, 64]
3	Polypyrrole (PPy) functionalized biochar (BC)	Fabricated utilizing freshly generated Fe^{3+}	Removed 17 distinct categories of PFAS (elimination > 94%)	Conventional pyrolysis temp: 501C°–950°C PFBA = 3.89 milli mol/g PFBS = 1.54 milli mol/g PFOA = 2.56 milli mol/g PFAS = 1.23 milli mol/g	34.8 m^2/g	[2]
4	Biosolids- derived biochar	Coated with CNM (carbon nanomaterials)	PFAS elimination efficacy: 79%	Pre-treated bio-solids were kept in a furnace (2.5 h.) Temp. = 900°C PFA = 310 μg L^{-1} 0.450 μm polyethersulfone membrane filter RPM = 180 Agitation time = 48 h.	—	[61]
5	Spent coffee grounds biochar	Templated MIP (molecularly imprinted polymers) was immobilized on spent coffee grounds biochar.	An acquired adsorbent material exhibits an enhanced capacity for the removal of per-fluoroalkyl acids (PFAAs) from aqueous solutions.	Thermogravimetric analysis was done at 25°C to 810°C.	1054 m^2/g	[65]

TABLE 4 | Comprehensive compilation of production and sorption parameters.

Sr. No.	Biomass type	Modification/pre-treatment	Biochar employed and processing parameters	Adsorption capacity	Removal efficiency	Sorption mechanism	Kinetic model/ adsorption isotherm used	References
1)	Biochar prepared from wood chips	The biochar was modified with a copolymer of sulfobetaine (SBMA) and acrylamide through water radical polymerization.	a) Pristine biochar prepared by slow pyrolysis of wood chips at 600°C for 2 h. b) Biochar-polymer composite (BC-P(SB-co-AM)) prepared by loading SBMA and acrylamide onto biochar followed by water radical Polymerization.	a) Maximum adsorption capacity for PFOS: 634 mg/g b) Maximum adsorption capacity for PFOA: 536 mg/g c) Maximum adsorption capacity for PFBS: 301 mg/g d) Maximum adsorption capacity for PFBA: 264 mg/g	a) Removal efficiency for PFOS: 99.7% b) Removal efficiency for PFOA: 98.3% c) Removal efficiency for PFBS: 95.2% d) Removal efficiency for PFBA: 92.8%	Hydrophobicity - interaction between hydrophobic moieties of PFAS and BC-P(SB-co-AM). Electrostatic attraction between cationic groups on the biochar and anionic PFAS molecules (affected by pH).	Pseudo 2nd order kinetic model	[1]
2)	The biochar used in the study was made from pine sawdust	The modification/pre-treatment involved the synthesis of $Fe_3O_4^-$ coated biochar followed by the etching of $Fe_3O_4^-$ coated biochar with concentrated HCl to incrementally liberate Fe^{3+} from the biochar surface.	Pine sawdust biochar was employed, and the processing parameters included pyrolytic decomposition at varying thermal conditions (500°C–900°C) to produce the biochar and chemical co-precipitation of Fe^{3+}/Fe^{2+} on biochar to synthesize Fe_3O_4-coated biochar.	The adsorption capacities of the PPy/BC composites were reported as (a) PFBA-3.88 mmol/g (b) PFBS-1.52 milli mol g^{-1}, for short-chain and (a) PFOA- 2.54 milli mol g^{-1} (b) PFOS- 1.23 milli mol g^{-1} for long-chain	The removal efficiency for 17 separate groups of PFAS was reported to be greater than 95%.	The sorption mechanism primarily stems from surface adsorption bolstered by electrostatic attractions.	The sorption kinetics were evaluated using the pseudo-second-order (PSO) model	[2]
3)	Leftover Karanja shells	Alteration of surface-bound functional moieties utilization of cetyltrimethylammonium bromide (CTAB).	Karanja shells, biomass-to-acid ratio 1:2.5, thermal condition of 450ºC, and a 1% cetyltrimethylammonium bromide (CTAB) solution	Maximum PFOA adsorption capacities exhibited by Karanja AC and CTAB K-AC were 157.1 mg/g & 455.8 mg/g, respectively	The adsorbent removed ~90% of PFOA	Multiple removal pathways including electrostatic, hydrophobic, ion-exchange, and hydrogen bonding interactions.	Thomas and Yoon Nelson model	[69]

(Continues)

TABLE 4 | (Continued)

Sr. No.	Biomass type	Modification/pre-treatment	Biochar employed and processing parameters	Adsorption capacity	Removal efficiency	Sorption mechanism	Kinetic model/ adsorption isotherm used	References
4)	Central part of corn, Oregon pine, eucalyptus, cottonwood, forage crop, and one industrial biochar	Ball milling was used to decrease particle size	Biochars were produced via slow pyrolysis at targeted temperatures in the range: Of 450°C–900°C	—	The removal efficiency of PFOS was assessed, with douglas fir 900, poplar 900, and the commercial biochar showing removal efficiencies of over 95%	The sorption mechanism involves physical and chemical sorption, particularly facilitated by the physiochemical attributes of biochar, including pore dimensions specific surface area (SSA), and hydrophobicity.	Linear regression models were used to analyze potential connections amongst pyrolysis temperature, biochar physicochemical properties, and removal of PFOS.	[68]
5)	Biochar made from biosolids via pyrolysis	Biosolids were made to 100–300 μm particle sizes and then pyrolyzed at 700°C for 3 hours.	Biochar was used as a catalyst for biogas decomposition at 900°C	—	The removal efficiency of PFAS using CNM-coated biochar was 79%	CNMs possess a porosity, high specific surface area, thermal and chemical stability, and anion-cation adsorption capacity, making them effective for PFAS removal	—	[61]
6)	Rice husk	Pyrolytic carbonization at 600°C for 2 h	Pristine biochar synthesized at 600°C through pyrolysis	—	The synthesized biochar showed 94% removal of EBT dye	Sorption of EBT dye onto the surface of biochar, facilitated by micropores	—	[70]
7)	Spent coffee grounds	Nitrogen functionalization via two methodologies of electrophilic aromatic substitution succeeded by reduction or thermally-catalyzed incorporation of melamine	The biochar derived from spent coffee grounds underwent functionalization through the introduction of surface-bound nitrogenous functional moieties. Subsequently,	C And BC-N@MIP-V: High PFOS sorption Kd values (1400 and 880 L g^{-1}) correspond to their high BET SSA (857 and 740 m^2 g^{-1}).	—	The sorption mechanism involved the selective adsorption of perfluoroalkyl acids (PFAAs), with specific	The text does not specify a particular kinetic model or adsorption isotherm used for the study. However, the adsorption	[70]

(Continues)

TABLE 4 | (Continued)

Sr. No.	Biomass type	Modification/pre-treatment	Biochar employed and processing parameters	Adsorption capacity	Removal efficiency	Sorption mechanism	Kinetic model/ adsorption isotherm used	References
			PFOS was immobilized onto the functionalized biochar surface via radical-initiated polymerization. VBTAC was employed as a functional monomer during the fabrication of the MIP.	BC-M@MIP-V: Low K_d value of 1.88 L g^{-1} with an increased aqueous content in equilibrium of PFOS.		functional monomers facilitating interaction with the target compounds	behavior was evaluated based on equilibrium adsorption and selectivity coefficients	
8)	The biochar was derived from sludge	Three different modification methods were applied to the biochar: acid, alkali, and oxidant modification	The biochar was prepared at a pyrolysis temperature of 300°C	Theoretical maximum adsorption capacities of the biochar for PFOS and perfluorooctanoic acid (PFOA) were quantified as 72.17 and 45.88 mg g^{-1}, respectively, through experimental analysis.	—	The adsorption mechanism involves hydrogen bonding, hydrophobic interaction, and electrostatic interaction between the biochar and PFAS	The kinetics of adsorption were delineated pseudo-second-order model, whereas adsorption isotherms conformed to the empirical data employing the dubinin-Radushkevich and Sips models	[71]
9)	Wood- derived biochar	—	Activated carbons and/or wood-derived biochar; processing parameters not specified.	—	Adsorption using activated carbons and/or wood-derived biochar achieved removal efficiencies of ~95–100%.	Hydrophobic interactions are the predominant mechanism accountable for the adsorption of PFAS onto biochar.	—	[72]
10)	Modified clay	Introducing quaternary [NH 4] + cations into the exchangeable interlayer sites of clay through intercalation.	Modified clay (Fluoro200) was employed. Processing parameters include adsorbent to solution ratios ranging from 4 to 50 mg dry modified clay: 450 mL water	—	Removal efficiency ranged from 95% to 99% for PFAS pollutants in groundwater	The mechanism of adsorption involves ionic interactions between the terminal oxygen atoms of carboxylate or	PFAS uptake using clay was characterized using piecewise isotherms. Specifically, both Langmuir and	[73]

(Continues)

TABLE 4 | (Continued)

Sr. No.	Biomass type	Modification/pre-treatment	Biochar employed and processing parameters	Adsorption capacity	Removal efficiency	Sorption mechanism	Kinetic model/ adsorption isotherm used	References
						sulfonate groups contained in perfluoroalkyl substances (PFAS) and the cationic intercalant (N+) ions. Additionally, fluorophilic attraction among PFASs further facilitates the adsorption process.	linear isotherms were discerned in the adsorption processes involving anionic and neutral PFASs. To accommodate the heterogeneity of interlayer surface sites, the modified Langmuir-Freundlich model was employed for analysis.	
11)	Pine- derived biochar	The biochar was produced at 750°C (P750)	—	The adsorption capacity was dependent on the PFAS blend and soil type. PFOS exhibited the highest adsorption capacity in loamy sand	The removal efficiency change was dependent on the PFAS blend, and soil type, with sandy clay loam showing higher removal efficiency compared to loamy sand for most compounds	The sorption mechanism was influenced by the physiochemical properties of the soil and the PFAS compound, with functional groups potentially playing a greater role than chain length	Kinetic data well fitted to the pseudo 2nd order model, and isothermal sorption modeling was not possible due to the high impact of soil fraction on initial sorption	[74]

(Continues)

TABLE 4 | (Continued)

Sr. No.	Biomass type	Modification/pre-treatment	Biochar employed and processing parameters	Adsorption capacity	Removal efficiency	Sorption mechanism	Kinetic model/ adsorption isotherm used	References
12)	Magnesium chloride- fortified biochar	Magnesium chloride (MgCl2) treatment	—	The sorption of PFASs to activated carbons (ACs) was high, with log K_d in between 0.9 and 5.1 for PFCAs and between 2.9 and 5.2 for PFSAs, FTSAs, and FOSA.	—	For shorter-chained per- and polyfluoroalkyl substances (PFASs), electrostatic sorption predominantly governed the adsorption process, whereas for longer-chained PFASs, hydrophobic sorption predominated.	The text refers to the utilization of an extensive array of sorbents evaluated for diverse per- and polyfluoroalkyl substances (PFASs) in batch sorption experiments conducted within a meticulously controlled experimental framework. However, it doesn't specify a particular kinetic model or adsorption isotherm used	[75]

employed as the precursor for biochar production, any modification or pre-treatment applied to the biomass, details regarding the biochar utilized, such as its source material and processing parameters, and the resultant adsorption capacity and removal efficiency of PFAS. Furthermore, insights into the sorption mechanism underlying PFAS adsorption onto biochar surfaces are provided, along with the specific kinetic models or adsorption isotherms employed to characterize the adsorption behavior [76].

8 | Adsorption Mechanisms

The distinctive attributes of biochar in adsorbing the PFAS are elucidated through its adsorption mechanisms, kinetics, and thermodynamics. The augmented surface area and porosity of biochar, are enhanced via physical and chemical modification methods. Physical methods such as ball milling provide numerous active sites for binding, acid modifications introduce oxygen-bearing functional moieties for cation exchange capacity, and alkali modifications facilitate π-π interactions. Kinetic studies reveal the adsorption of PFAS involvement in pseudo-first, second-order kinetic models. For instance, the pseudo-2nd-order kinetic model is indicative of chemisorption involving valence forces. Thermodynamic analyses demonstrate the endothermic and spontaneous adsorption process. These synergistic properties render biochar an exceptionally efficacious material for the adsorption and removal of PFAS from wastewater.

8.1 | Adsorption Kinetics

Adsorption kinetics involves examining how quickly adsorption occurs at which particles stick to the surface and the amount of time needed. A mechanism consisting of three consecutive steps can be used to define the total adsorption procedure on porous adsorbents. The 1st phase is intraparticle diffusion; The 2nd stage involves film diffusion, while the third step pertains to reaching equilibrium, characterized by the adsorption of adsorptive molecules onto the active sites of the porous adsorbent [77]. Table 5 illustrates the kinetics of adsorption processes through various models provided in the table. It offers a concise overview of the kinetic models utilized in research on the adsorption of per- and polyfluoroalkyl compounds (PFAS) onto biochar surfaces. Each table entry presents a distinct mathematical equation representing a kinetic model utilized to elucidate the temporal rate of PFAS adsorption onto the biochar surface over time. Various adsorption kinetic models have been developed to characterize the adsorption kinetic process, including the pseudo 1st order (PFO) model, pseudo-second-order (PSO) model, Ritchie's equation (RE), mixed-order (MO) model the Elovich model (EM), and phenomenological mass transfer models. The table below (Table 5) lists these adsorption kinetic models along with their respective equations.

8.2 | Adsorption Isotherm

Adsorption isotherm models are essential tools in adsorption processes, offering crucial insights pertaining to the interaction between adsorbate and adsorbent under equilibrium conditions and isothermal circumstances. They play a fundamental role in understanding solute-adsorbent interactions and improving their utilization. Innumerable models are employed to correlate experimental data, with the best-fitting model providing valuable information on adsorption behavior. While These methods elucidate underlying adsorption mechanisms and assist in designing efficient adsorption systems. Isotherm models also offer insights into maximum adsorption capacity, crucial for evaluating adsorbent performance. Several models, including linear, Freundlich, Sips, Langmuir, and Brunauer, Emmett, and Teller (BET) models, are utilized to investigate adsorption mechanisms across different systems, each providing unique perspectives on adsorption behavior and contributing to a comprehensive understanding of adsorption processes [80]. Table 6 below offers a concise summary of the isotherm models utilized in studies investigating the adsorption of per- and polyfluoroalkyl compounds (PFAS) onto biochar surfaces. Each entry in the table details the specific mathematical equation representing the isotherm model employed, along with its classification (e.g., Langmuir, Freundlich). Additionally, a brief description of the significance of each isotherm model is provided, outlining its applicability and limitations in elucidating the adsorption behavior of PFAS onto biochar.

8.3 | Adsorption Thermodynamic Studies

Thermodynamic of adsorption—The Van't Hoff plot is utilized to examine thermodynamic properties like free enthalpy (ΔH°), free entropy (ΔS°), and Gibbs free energy change (ΔG°), offering

TABLE 5 | Adsorption kinetic models and their respective equations.

Sr no.	Kinetic model	Equation	Significance	References
1.	Pseudo 1st order	$\ln(q_t - q_c) = \ln q_e - k_{1t}$	Postulated that the rate of adsorption site occupation is directly proportional to the number of unoccupied sites	[78]
2.	Pseudo 2nd order	$\frac{t}{q_t} = \frac{1}{k_2 q_e^2} + \frac{t}{q_e}$	The adsorption process depends on the availability of adsorption sites	[78]
3.	Elovich model	$q_t = \frac{1}{\beta}(\alpha\beta) + \frac{1}{\beta}\ln t$	Chemisorption process on highly heterogeneous surface	[79]
4.	Intra-particle diffusion model	$q_t = k_i\ t^{1/2} + C'$	Consider inter-particle diffusion mechanisms	[79]

TABLE 6 | Adsorption isotherm models and their equations. Reprinted with permission from [81]. Copyright 2023, American Institute of Physics.

Sr. no	Isotherm model	Equation	Type of isotherm	Significance
1.	Langmuir model	$\frac{C_e}{q_e} = \frac{C_e}{Q_m} + \frac{1}{Q_m b}$	Two-parameter model	Langmuir's theory describes adsorption equilibrium with a single, uniform-energy monolayer formed by non-interacting molecules.
2.	Freundlich adsorption isotherm	$\log q_e = \log k_f + \frac{1}{n}\log C_e$	Two-parameter model	Freundlich isotherm describes multilayered adsorption on heterogeneous surfaces with an exponential distribution of site energies.
3.	Langmuir– Freundlich adsorption isotherm	$q_e = \frac{Q_{LFM}(k_{LFC_e})M_{LF}}{1 + (k_{LFC_e})M_{LF}}$	Two-parameter model	This adsorption isotherm model elucidates the dissemination of sorption energy across the heterogeneous sites of the absorbent. At diminished adsorbate concentrations, the isotherm adheres to the freundlich model, whereas at augmented adsorbate concentrations, it transitions to the Langmuir model.
4.	Temkin model	$q_e = \frac{RT}{b_T}\ln A_T + \frac{RT}{b}\ln C_e$	Two-parameter model	This isotherm analyses chemisorption on heterogeneous surfaces, considering adsorbate-adsorbent interactions and a linear decrease in heat with coverage.
5.	Brunauer–Emmett–Teller (BET) model	$q_e = \frac{q_s C_{BET} C_e}{(C_s - C_e)[1 + (C_{BET} - 1)\left(\frac{C_e}{C_s}\right)}$	Two-parameter mode	BET isotherm describes gas-solid adsorption with multilayers for pressures between 0.05 and 0.3 P/Po, used for surface area determination via nitrogen sorption.
6	Dubinin–Radushkevich (D– R) isotherm mode	$q_e = q_{max} e^{(-\beta' \varepsilon^2)}$	Two-parameter mode	The D-R isotherm focuses on micropore filling in heterogeneous materials, explaining adsorption by a Gaussian energy distribution, not layer-by-layer filling.
7	Redlich peterson model	$q_e = \frac{k_R C_e}{1 + a_R C_e^g}$	Three-parameter model	The Langmuir-freundlich isotherm combines Langmuir and freundlich models for heterogeneous or homogeneous systems, mimicking the Henry's law region at low concentrations.
8.	Sips isotherm model	$q_e = \frac{q_m (k_s C_e)^m}{[1 + (k_s C_e)^m]}$	Three-parameter model	This model integrates the freundlich and Langmuir adsorption isotherms, addressing the limitations associated with high adsorbate concentrations in the freundlich model while accounting for the heterogeneity of sorption sites. It formulates mathematical expressions with finite bounds at elevated concentrations. This isotherm effectively limits adsorption without interactions among adsorbates. It deviates from Henry's law due to its reduction to the freundlich model at low adsorbate concentrations. However, at higher adsorbate concentrations, it predicts the monolayer adsorption characteristics indicative of the Langmuir model.

an understanding into the spontaneity of the adsorption process [82]. Equations (2) and (3) are utilized for conducting an analysis related to the adsorption process, specifically focusing on the distribution coefficient (K_d) and its relationship with temperature.

$$\ln K_d = \frac{\Delta S^\circ}{R} - \frac{\Delta H^\circ}{RT} \quad (2)$$

$$K_d = \frac{q_e}{C_e} \quad (3)$$

R = Universal gas constant

T = absolute temperature (K)

The ln K_d versus 1/T plot serves to determine the ΔH° and ΔS° values Subsequently, the Gibbs free energy change (ΔG°) is computed using

$$\Delta G^\circ = \Delta H^\circ - T\Delta S^\circ \quad (4)$$

ΔG° is Gibbs free energy change, ΔH° is enthalpy change, ΔS° is entropy change, and T is temperature [83].

Table 7 provides a description of various processes indicating their spontaneity, the range of parameters involved, the magnitude of selected parameters, and the adsorption thermodynamics. Table 8 summarizes various AI and ML techniques, including their applications, advantages, and limitations, in the context of wastewater treatment and monitoring.

9 | Theoretical Study for Predicting the Removal of PFAS Using Biochar-Based Adsorbent

Machine learning (ML) is a subfield of artificial intelligence (AI) concerned with emerging algorithms that can learn without explicit programming from data. Unlike traditional programming where rules are predefined, ML algorithms identify patterns and relationships within historical datasets. This ability to learn and adapt makes ML particularly valuable in complex water applications where traditional methods struggle with intricate data and changing conditions. The core strength of machine learning in water treatment lies in its exceptional ability to identify correlations within complex datasets, even when the underlying mathematical relationships are not fully understood. This allows ML models to predict water treatment behavior, such as optimal chlorination dosage or membrane filtration efficiency, based on historical data and identified patterns. Additionally, ML's adaptability allows it to learn from new data as it becomes available, continuously improving its models and performance over time. This is crucial for water systems that need to adapt to dynamic water quality or environmental conditions. Finally, ML models can be generalized to new situations beyond the specific data they were trained on, offering cost savings and process optimization across different water treatment plants or natural water systems. The following table no. 8, succinctly encapsulates various artificial intelligence (AI) and machine learning (ML) models and practices [84]. The artificial intelligence methodologies, encompassing ANN (Artificial Neural Networks), Support Vector Machines (SVM), and Adaptive Neuro-Fuzzy Inference Systems (ANFIS), have exhibited accomplished predictive competence in the realm of adsorption process estimation, adsorption capacity, and efficiency of biochar [85].

Neural networks, Support vector machines, and tree-based approaches are examples of algorithms in machine learning that have become potent tools for constructing predictive models for adsorption. These algorithms excel in unveiling intricate nonlinear relationships within data, resulting in more precise predictions compared to conventional regression methods like multilinear regression (MLR). Multilinear Regression (MLR) Model, a prevalent technique in poly parameter linear free energy relationships (pp-LFERs), is utilized to correlate the adsorption coefficient (log K_d) with adsorbate properties and it is represented by the Equation (5).

$$\log K_d(c_e) = e.\,E + s.\,S + a.\,A + b.\,B + v.\,V + c \quad (5)$$

where,

log K_d = adsorption coefficient (1/cm)

(C_e) = Adsorption coefficient

(E, S, A, B, V) = Abraham descriptors for the adsorbate

(e, s, a, b, v, c) = fitting parameters

This equation facilitates the correlation of (log K_d) with various adsorbate properties. However, it necessitates a distinct MLR model for each equilibrium concentration level, thereby limiting its predictive capacity.

Neural networks comprise input, multiple hidden, and output layers, with optimization techniques like backpropagation employed during training to adjust the nodes' weights. Regularization strategies such as early halting are utilized to prevent overfitting, and grid search is conducted to optimize hyperparameters for the best model configuration. Shapley values analysis is employed to interpret the models by quantifying the contribution of each input variable. This analysis underscores

TABLE 7 | Significance of various adsorption thermodynamics parameters.

Adsorption thermodynamic parameter	The range of parameters selected	The magnitude of a selected parameter	Inference
Standard gibbs free energy ΔG0	ΔG0 < 0		Spontaneous process
	ΔG0 > 0		Non–Spontaneous process
Standard change in enthalpy ΔH°	ΔH° < 0	≤ 60 KJ/Mol = physisorption	Exothermic process
	ΔH° > 0	≥ 200 KJ/Mol = chemisorption	Endothermic process
Standard change in entropy ΔS°	ΔS° < 0		Lower degree of randomness
	ΔS° > 0		Higher degree of randomness

TABLE 8 | A synopsis of AI techniques and machine learning models employed in wastewater treatment and monitoring.

Monitoring applications and reviewed water treatment	Modeling and technique	General applications	Positive outcomes	Negative outcomes	References
• Membrane-process parameter modeling • Dissolved-oxygen-concentration modeling • Adsorption process parameter modeling	Artificial neural network (ANN)-General	• Regression, classification • (Typically) Supervised machine learning	• Forward propagation capable of cheap and fast computation • Capable of handling high-dimensional datasets • Modeling/prediction results are relatively fast	• Some models and architectures are difficult to understand. • High computational power required	[86–88]
• Aquaponics growth stage classification	k-Nearest Neighbor (k-NN)	• Classification • Administered machine learning	• Possessing the capacity to assimilate novel data incorporations. • Simple to implement with minimal or no required training period.	• Prone to perturbations, data omissions, and anomalous deviations. • Poor performance with large datasets	[86, 89, 90]
• Dissolved-oxygen-concentration modeling	Hammerstein-Wiener (HW)	• Regression • Machine-learning model	• Inherent non-linearities can be nullified to facilitate the application of linear computational methodologies. • Adept at constructing models for dynamic datasets exhibiting intrinsic static non-linear characteristics	• An exceptionally intricate model that poses significant challenges in both comprehensive and implementation.	[91–95]
• Membrane-process parameter modeling • Adsorption process removal efficiency • DBP formation modeling	Radial basis function (RBF) kernel	• Regression, classification • Machine-learning function	• Capable of handling noisy datasets • Exhibits superior computational efficiency, operating with reduced processing power compared to conventional ANN models. • Less susceptible to local minima/maxima issues	• Difficulty handling increasingly non-linear datasets. • The intricacy of the model escalates substantially with the augmentation of neurons within its singular hidden layer.	[86, 96–98]
• Dissolve oxygen concentration modeling • Membrane-process parameter modeling	Recurrent neural network (RNN) or long short-term memory (LSTM)	• Regression, Classification • Supervised machine learning	• Suitable for modeling and sequential datasets • There is no restriction on the length of dataset inputs. • Well-suited for time-series datasets and modeling.	• Needs high computational power • Training becomes challenging due to the necessity for extensive and diverse datasets.	[86, 99–102]

(Continues)

TABLE 8 | (Continued)

Monitoring applications and reviewed water treatment	Modeling and technique	General applications	Positive outcomes	Negative outcomes	References
• DBP formation modeling	CNN (convolutional neural network)	• Classification, regression, Segmentation • Supervised machine learning	• Results are characteristically observed as extremely precise • When the model operates concurrently, outcomes are swiftly ascertained. • Excel at solving with image-based inputs	• The model and its architectural framework are inherently intricate and expansive. • Involves high computational power	[86, 103–106]
• Dissolved-oxygen-concentration modeling	ELM (extreme learning machine)	• Supervised machine learning • Regression, classification	• Suitable for pattern classifications • Relatively short training times	It frequently encounters issues of overfitting or underfitting when there are excessive or insufficient data.	[107–109]

the significance of incorporating equilibrium concentration and adsorbent properties, challenging the oversimplified assumptions of earlier models. The developed machine learning models take into account both adsorbent and adsorbate characteristics, resulting in enhanced prediction capability. They are made accessible through user-friendly graphical interfaces, thereby enhancing their usability in adsorption research. In assumption, the amalgamation of machine learning techniques, particularly neural networks, with equations like the MLR model and pp-LFERs (Polyparameter Linear Free Energy Relationships) enables more accurate predictions of adsorption coefficients. These models consider a broad range of factors, including adsorbent properties, equilibrium concentration, and adsorbate characteristics, leading to notable advancements in adsorption research, The ANN model predicts the amount of chemical adsorption for a specific adsorbent-chemical combination based on the input data (chemical descriptors and adsorbent properties) [110]. Karbassiyazdi et al. examined the effectiveness of the XGBoost model as a proficient machine learning technique for the removal of PFAS. There is a need for advanced methods and materials, especially for short-chain PFAS not removed well by conventional methods. The objective of the study was applying machine learning with literature data to envisage PFAS removal factors for diverse adsorbents, improving material selection and process optimization. The methodology followed was that the Collected data on 234 PFAS removals from 64 published papers on adsorbents like activated carbon, resins, membranes. XGBoost model was used which handles missing data well and avoids overfitting. The Model predicts adsorption capacity (q_e), equilibrium time (t_e), and removal % (R) based on adsorbent type, particle size, concentrations, pH, etc. The equations for adsorption capacity and removal percentage is given by Equations (6) and (7).

Key equations:

$$q_e = (C_o - C_e)\, v/m \text{ (adsorption capacity)} \quad (6)$$

$$\text{removal}\% = (C_o - C_e)/C_o \times 100 \text{ (removal percentage)} \quad (7)$$

q_e: Adsorption capacity at equilibrium

C_o: Adsorbate Initial concentration

C_e: Adsorbate concentration

V: Solution or gas phase Volume

m: Adsorbent mass

- Compared feature importance and used SHAP values to interpret the model.

The findings of the work were particle size and pH are the most influential factors for PFAS exclusion predictions. Adsorbent type is important for q_e, while initial concentrations impact R%. Ion exchange resins and activated carbons showed the highest q_e. The Model has good performance based on RMSE and AUC scores. Machine learning can reliably estimate PFAS removal by adsorbents using process conditions as input. Model interpretations have revealed the dominant factors thus the

approach can be extended to other micropollutants and provides a framework for adsorbent design [111].

One of the studies includes peanut husk-derived biochar used for the adsorptive removal of PFAs and integrates the AI models to interpret the data obtained. Specifically, ANNs, SVM, and ANFIS were adapted to predict the optimal conditions for adsorption by analyzing datasets. ANN was used to stimulate the efficacy of PFOA removal was evaluated using an experimental dataset. The root mean square error values were computed for three distinct transfer functions, with the *tansig* transfer function yielding minimal RMSE values. The SVM model estimated the removal efficiency, leveraging RMSE and R^2 values, with experiments conducted on MATLAB, resulting in an execution time of 63.5 s. The root mean square error value of 11.40 and the coefficient of determination (R^2) value of 0.920. Simultaneously, the Adaptive Neuro-Fuzzy Inference System model was used for determining the correlation between the experimental and predicted data, revealing a higher R^2 value of 0.99 and an RMSE value of 0.50. This is empirical evidence of the robustness of the fuzzy inference system network in predicting PFOA elimination. Ultimately, the ANFIS and ANN models exhibited superior accuracy in removal efficiency prediction having an R^2 value of 0.99 whereas, the SVM model displayed relatively weaker predictive capabilities with an R^2 value of 0.920. Therefore, Machine learning significantly enhances the detection and adsorption capacities of modified biochar for PFAS. By employing advanced algorithms researchers could predict the PFOA or PFAS elimination. These models analyze the influence of surface properties and environmental factors, enabling the optimization of biochar modifications to maximize PFAS sequestration. Machine learning facilitates the rapid identification of key variables affecting the adsorption, thereby streamlining the development of more effective biochar [112].

10 | Conclusion and Future Prospects

This comprehensive review highlights biochar's potential as an effective solution for addressing PFAS water contamination. Biochar adsorption represents a highly promising and environmentally friendly approach to mitigating PFAS contamination, which poses significant toxicity risks to various organisms. A comprehensive examination of the toxicological ramifications of PFAS on both environmental and human health, alongside their environmental persistence, has been elucidated. Additionally, an evaluative review of the hazard index has been incorporated that provides a comprehensive assessment of the cumulative health risks posed by mixtures of PFAS. The modifications of biochar, particularly through treatments such as HCl, HNO_3, or $FeCl_3$ greatly enhance its adsorption capacity. These modifications of biochar are bifurcated into two principal categories: Physical and Chemical modifications. A thorough analysis of a few case studies encompassing various modified biochar whose adsorption capacities varied in the range of 79%–99.7% thus providing a wide spectrum of biochar and their analysis. A comprehensive study underlying adsorption isotherms, kinetics, and thermodynamics offers crucial insights into how PFAS interact with biochar while providing insight into the governing adsorption mechanisms, equilibrium time, and spontaneity, feasibility of the adsorption process, respectively. Utilizing machine learning models shows promise in predicting PFAS removal rates based on various process factors like adsorbent and adsorbate characteristics. Machine learning Models provide a panoptic view for predicting and analyzing the PFAS adsorption process and mechanism for further studies. This review serves as a comprehensive resource for developing optimized biochar-based solutions for sustainable and scalable treatment of PFAS-contaminated water.

Acknowledgments

The authors express their gratitude to Dr. C. P. Ramanarayanan, the Vice-Chancellor of DIAT (DU), Pune, for his unwavering encouragement and support. The first author acknowledges, Prof. Dr. Varsha Kulkarni, HOD Microbiology, STES's Sinhgad College of Science, Pune, Maharashtra. The authors would also like to thank Ms. Neelaambhigai Mayilswamy, Ms.Niranjana J.P, Ms. Alsha Subhash, Mr: Jigar Patadiya and Ms. Shruti Gupta for offering essential technical help and direction throughout the writing of review article.

Conflicts of Interest

The authors declare no conflicts of interest.

Data Availability Statement

Data sharing is not applicable to this article as no new data were created or analyzed in this study.

References

1. J. Deng, J. Han, C. Hou, et al., "Efficient Removal of Per- and Polyfluoroalkyl Substances From Biochar Composites: Cyclic Adsorption and Spent Regenerant Degradation," *Chemosphere* 341 (2023): 140051, https://doi.org/10.1016/j.chemosphere.2023.140051.

2. H. Yu, H. Chen, P. Zhang, et al., "In Situ Self-Sacrificial Synthesis of Polypyrrole/biochar Composites for Efficiently Removing Short- and Long-Chain Perfluoroalkyl Acid From Contaminated Water," *Journal of Environmental Management* 344 (2023): 118745, https://doi.org/10.1016/j.jenvman.2023.118745.

3. J. S. Boone, C. Vigo, T. Boone, et al., "Per- and Polyfluoroalkyl Substances in Source and Treated Drinking Waters of the United States," *Science of The Total Environment* 653 (2019): 359–369, https://doi.org/10.1016/j.scitotenv.2018.10.245.

4. M. D. Nguyen, A. K. Sivaram, M. Megharaj, et al., "Investigation on Removal of Perfluorooctanoic Acid (PFOA), Perfluorooctane Sulfonate (PFOS), Perfluorohexane Sulfonate (PFHxS) Using Water Treatment Sludge and Biochar," *Chemosphere* 338 (2023): 139412, https://doi.org/10.1016/j.chemosphere.2023.139412.

5. K. L. Smalling, K. M. Romanok, P. M. Bradley, et al., "Per- and Polyfluoroalkyl Substances (PFAS) in United States Tapwater: Comparison of Underserved Private-Well and Public-Supply Exposures and Associated Health Implications," *Environment International* 178 (2023): 108033, https://doi.org/10.1016/j.envint.2023.108033.

6. S. Kurwadkar, J. Dane, S. R. Kanel, et al., "Per- and Polyfluoroalkyl Substances in Water and Wastewater: A Critical Review of Their Global Occurrence and Distribution," *Science of The Total Environment* 809 (2022): 151003, https://doi.org/10.1016/j.scitotenv.2021.151003.

7. J. C. Francis, A. Nighojkar, and B. Kandasubramanian, "Relevance of Wood Biochar on CO2 Adsorption: A Review," *Hybrid Advances* 3 (2023): 100056, https://doi.org/10.1016/j.hybadv.2023.100056.

8. A. Kalla, N. Mayilswamy, B. Kandasubramanian, and P. Mahajan-Tatpate, "Biochar: A Sustainable and an Eco-Friendly Material for Energy Storage Applications," *International Journal of Green Energy* 21, no. 7 (2024): 1695–1709, https://doi.org/10.1080/15435075.2023.2259973.

9. S. R. Kulkarni, A. Nighojkar, and B. Kandasubramanian, "Aqueous Adsorption of Pharmaceutical Pollutants on Biochar: A Review on Physicochemical Characteristics, Classical Sorption Models, and Advancements in Machine Learning Techniques," *Water, Air, and Soil Pollution* 234, no. 11 (2023): 684, https://doi.org/10.1007/s11270-023-06696-9.

10. S. S. Kulkarni, N. Mayilswamy, S. Sidharth, A. Subash, A. Satapathy, and B. Kandasubramanian, "Sustainable Wastewater Management Via Biochar Derived From Industrial Sewage Sludge," *Circular Economy and Sustainability* 4, no. 1 (2024): 163–200, https://doi.org/10.1007/s43615-023-00273-2.

11. P. Sangrulkar, S. Gupta, and B. Kandasubramanian, "Advancements in Biochar-Based Electrodes for Improved Performance of Microbial Fuel Cells," *Bioresource Technology Reports* 24 (2023): 101684, https://doi.org/10.1016/j.biteb.2023.101684.

12. P. Gole, K. Raut, and B. Kandasubramanian, "Polymer-based Biochar Materials for Environmental Remediation: A Review," *Hybrid Advances* 6 (2024): 100267, https://doi.org/10.1016/j.hybadv.2024.100267.

13. N. Mayilswamy, A. Nighojkar, M. Edirisinghe, S. Sundaram, and B. Kandasubramanian, "Sludge-derived Biochar: Physicochemical Characteristics for Environmental Remediation," *Applied Physics Reviews* 10, no. 3 (2023), https://doi.org/10.1063/5.0137651.

14. D. Damahe, N. Mayilswamy, and B. Kandasubramanian, "Biochar/metal Nanoparticles-Based Composites for Dye Remediation: A Review," *Hybrid Advances* 6 (2024): 100254, https://doi.org/10.1016/j.hybadv.2024.100254.

15. A. Ayalew, R. R. Gonte, and K. Balasubramanian, "Development of Polymer Composite Beads for Dye Adsorption," *International Journal of Green Nanotechnology* 4 (2012): 440–454, https://doi.org/10.1080/19430892.2012.739480.

16. R. R. Gonte, G. Shelar, and K. Balasubramanian, "Polymer–Agro-Waste Composites for Removal of Congo Red Dye From Wastewater: Adsorption Isotherms and Kinetics," *Desalination and Water Treatment* 52, no. 40-42 (2014): 7797–7811, https://doi.org/10.1080/19443994.2013.833876.

17. N. Mayilswamy and B. Kandasubramanian, *Various Biomasses from Wastewater and Possibilities of Conversion to Energy Resources* (Beverly, MA: Scrivener Publishing, Wiley, 2024), 259.

18. A. Nighojkar, S. Pandey, M. Naebe, et al., "Using Machine Learning to Predict the Efficiency of Biochar in Pesticide Remediation," *NPJ Sustainable Agriculture* 1 (2023): 1, https://doi.org/10.1038/s44264-023-00001-1.

19. F. Dixit, G. Munoz, M. Mirzaei, et al., "Removal of Zwitterionic PFAS by MXenes: Comparisons With Anionic, Nonionic, and PFAS-Specific Resins," *Environmental Science & Technology* 56, no. 10 (2022): 6212–6222, https://doi.org/10.1021/acs.est.1c03780.

20. M. Nannaware, N. Mayilswamy, and B. Kandasubramanian, "PFAS: Exploration of Neurotoxicity and Environmental Impact," *Environmental Science and Pollution Research* 31, no. 9 (2024): 12815–12831, https://doi.org/10.1007/s11356-024-32082-x.

21. A. Ramírez Carnero, A. Lestido-Cardama, P. Vazquez Loureiro, L. Barbosa-Pereira, A. Rodríguez Bernaldo de Quirós, and R. Sendón, "Presence of Perfluoroalkyl and Polyfluoroalkyl Substances (PFAS) in Food Contact Materials (FCM) and its Migration to Food," *Foods* 10, no. 7 (2021): 1443, https://doi.org/10.3390/foods10071443.

22. S. E. Fenton, A. Ducatman, A. Boobis, et al., "Per- and Polyfluoroalkyl Substance Toxicity and Human Health Review: Current State of Knowledge and Strategies for Informing Future Research," *Environmental Toxicology & Chemistry* 40, no. 3 (2021): 606–630, https://doi.org/10.1002/etc.4890.

23. B. Saawarn, B. Mahanty, and S. Hait, "Adsorptive Removal of Perfluorooctanoic Acid From Aqueous Matrices Using Peanut Husk-Derived Magnetic Biochar: Statistical and Artificial Intelligence Approaches, Kinetics, Isotherm, and Thermodynamics," *Chemosphere* 360 (2024): 142397, https://doi.org/10.1016/j.chemosphere.2024.142397.

24. S. E. Fenton, A. Ducatman, A. Boobis, et al., "Per- and Polyfluoroalkyl Substance Toxicity and Human Health Review: Current State of Knowledge and Strategies for Informing Future Research," *Environmental Toxicology & Chemistry* 40, no. 3 (2021): 606–630, https://doi.org/10.1002/etc.4890.

25. H. Brunn, G. Arnold, W. Körner, G. Rippen, K. G. Steinhäuser, and I. Valentin, "PFAS: Forever Chemicals—Persistent, Bioaccumulative and Mobile. Reviewing the Status and the Need for Their Phase Out and Remediation of Contaminated Sites," *Environmental Sciences Europe* 35, no. 1 (2023): 20, https://doi.org/10.1186/s12302-023-00721-8.

26. J. McAdam and E. M. Bell, "Determinants of Maternal and Neonatal PFAS Concentrations: A Review," *Environmental Health* 22, no. 1 (2023): 41, https://doi.org/10.1186/s12940-023-00992-x.

27. Q. Zhang, Y. Wang, X. Shen, et al., "Environmental Exposure to Per- and Perfluoroalkyl Substances in Early Pregnancy and Newborn Anogenital Distance: A Prospective Cohort Study," *Environmental Science and Pollution Research* 30, no. 44 (2023): 99704–99712, https://doi.org/10.1007/s11356-023-29446-0.

28. H. Brunn, G. Arnold, W. Körner, G. Rippen, K. G. Steinhäuser, and I. Valentin, "PFAS: Forever Chemicals—Persistent, Bioaccumulative and Mobile. Reviewing the Status and the Need for Their Phase Out and Remediation of Contaminated Sites," *Environmental Sciences Europe* 35, no. 1 (2023): 20, https://doi.org/10.1186/s12302-023-00721-8.

29. E. M. Sunderland, X. C. Hu, C. Dassuncao, A. K. Tokranov, C. C. Wagner, and J. G. Allen, "A Review of the Pathways of Human Exposure to Poly- and Perfluoroalkyl Substances (PFASs) and Present Understanding of Health Effects," *Journal of Exposure Science and Environmental Epidemiology* 29, no. 2 (2019): 131–147, https://doi.org/10.1038/s41370-018-0094-1.

30. A. Mojiri, M. Nazari Vishkaei, H. K. Ansari, M. Vakili, H. Farraji, and N. Kasmuri, "Toxicity Effects of Perfluorooctanoic Acid (PFOA) and Perfluorooctane Sulfonate (PFOS) on Two Green Microalgae Species," *International Journal of Molecular Sciences* 24, no. 3 (2023): 2446, https://doi.org/10.3390/ijms24032446.

31. Z. Niu, J. Na, W. Xu, N. Wu, and Y. Zhang, "The Effect of Environmentally Relevant Emerging Per- and Polyfluoroalkyl Substances on the Growth and Antioxidant Response in Marine Chlorella Sp," *Environmental Pollution* 252 (2019): 103–109, https://doi.org/10.1016/j.envpol.2019.05.103.

32. H. M. Starnes, K. D. Rock, T. W. Jackson, and S. M. Belcher, "A Critical Review and Meta-Analysis of Impacts of Per- and Polyfluorinated Substances on the Brain and Behavior," *Frontiers in Toxicology* 4 (2022), https://doi.org/10.3389/ftox.2022.881584.

33. C. Liu, K. Y. H. Gin, and V. W. C. Chang, "Multi-biomarker Responses in Green Mussels Exposed to PFCs: Effects at Molecular, Cellular, and Physiological Levels," *Environmental Science and Pollution Research* 21, no. 4 (2014): 2785–2794, https://doi.org/10.1007/s11356-013-2216-6.

34. T. Ma, C. Ye, T. Wang, X. Li, and Y. Luo, "Toxicity of Per- and Polyfluoroalkyl Substances to Aquatic Invertebrates, Planktons, and Microorganisms," *International Journal of Environmental Research and Public Health* 19, no. 24 (2022): 16729, https://doi.org/10.3390/ijerph192416729.

35. X. B. Wen, L. Q. Chen, Z. L. Zhou, C. X. Ai, and G. Y. Deng, "Reproduction Response of Chinese Mitten-Handed Crab (Eriocheir Sinensis) Fed Different Sources of Dietary Lipid," *Comparative Biochemistry and Physiology Part A: Molecular & Integrative Physiology*

131, no. 3 (2002): 675–681, https://doi.org/10.1016/s1095-6433(01)00515-3.

36. G. Ding, L. Wang, J. Zhang, et al., "Toxicity and DNA Methylation Changes Induced by Perfluorooctane Sulfonate (PFOS) in Sea Urchin Glyptocidaris Crenularis," *Chemosphere* 128 (2015): 225–230, https://doi.org/10.1016/j.chemosphere.2015.01.045.

37. R. Qu, J. Liu, L. Wang, and Z. Wang, "The Toxic Effect and Bioaccumulation in Aquatic Oligochaete Limnodrilus Hoffmeisteri After Combined Exposure to Cadmium and Perfluorooctane Sulfonate at Different pH Values," *Chemosphere* 152 (2016): 496–502, https://doi.org/10.1016/j.chemosphere.2016.03.024.

38. K. Ji, Y. Kim, S. Oh, B. Ahn, H. Jo, and K. Choi, "Toxicity of Perfluorooctane Sulfonic Acid and Perfluorooctanoic Acid on Freshwater Macroinvertebrates (*Daphnia Magna and Moina macrocopa*) and Fish (*Oryzias latipes*)," *Environmental Toxicology & Chemistry* 27, no. 10 (2008): 2159–2168, https://doi.org/10.1897/07-523.1.

39. L. Zhang, J. Niu, Y. Wang, J. Shi, and Q. Huang, "Chronic Effects of PFOA and PFOS on Sexual Reproduction of Freshwater Rotifer Brachionus Calyciflorus," *Chemosphere* 114 (2014): 114–120, https://doi.org/10.1016/j.chemosphere.2014.03.099.

40. W. Liu, S. Chen, X. Quan, and Y. Jin *Environmental Toxicology & Chemistry* preprint, no. 2008 (2007): 1, https://doi.org/10.1897/07-459.

41. W. Liu, Y.-B. Zhang, X. Quan, Y.-H. Jin, and S. Chen, "Effect of Perfluorooctane Sulfonate on Toxicity and Cell Uptake of Other Compounds With Different Hydrophobicity in Green Alga," *Chemosphere* 75, no. 3 (2009): 405–409, https://doi.org/10.1016/j.chemosphere.2008.11.084.

42. D. Xu, X. Chen, and B. Shao, "Oxidative Damage and Cytotoxicity of Perfluorooctane Sulfonate on Chlorella Vulgaris," *Bulletin of Environmental Contamination and Toxicology* 98, no. 1 (2017): 127–132, https://doi.org/10.1007/s00128-016-1957-6.

43. R. Rosal, I. Rodea-Palomares, K. Boltes, F. Fernández-Piñas, F. Leganés, and A. Petre, "Ecotoxicological Assessment of Surfactants in the Aquatic Environment: Combined Toxicity of Docusate Sodium With Chlorinated Pollutants," *Chemosphere* 81, no. 2 (2010): 288–293, https://doi.org/10.1016/j.chemosphere.2010.05.050.

44. N. T. Hayman, G. Rosen, M. A. Colvin, J. Conder, and J. A. Arblaster, "Aquatic Toxicity Evaluations of PFOS and PFOA for Five Standard Marine Endpoints," *Chemosphere* 273 (2021): 129699, https://doi.org/10.1016/j.chemosphere.2021.129699.

45. P. Logeshwaran, A. K. Sivaram, A. Surapaneni, K. Kannan, R. Naidu, and M. Megharaj, "Exposure to Perfluorooctanesulfonate (PFOS) but Not Perfluorooctanoic Acid (PFOA) at Ppb Concentration Induces Chronic Toxicity in Daphnia Carinata," *Science of The Total Environment* 769 (2021): 144577, https://doi.org/10.1016/j.scitotenv.2020.144577.

46. R. W. Flynn, M. F. Chislock, M. E. Gannon, et al., "Acute and Chronic Effects of Perfluoroalkyl Substance Mixtures on Larval American Bullfrogs (Rana catesbeiana)," *Chemosphere* 236 (2019): 124350, https://doi.org/10.1016/j.chemosphere.2019.124350.

47. B. Barua, L. K. Dunham, A. Gadh, and S. Savagatrup, "Real-time Detection and Classification of PFAS Using Dynamic Behaviors at Liquid–Liquid Interfaces," *RSC Applied Interfaces* 1, no. 5 (2024): 1045–1056, https://doi.org/10.1039/d4lf00128a.

48. S. Y. Wee and A. Z. Aris, "Revisiting the 'Forever Chemicals', PFOA and PFOS Exposure in Drinking Water," *NPJ Clean Water* 6, no. 1 (2023): 57, https://doi.org/10.1038/s41545-023-00274-6.

49. B. D. Etz and M. K. Shukla, "Per- and Polyfluoroalkyl Substances Chemical Degradation Strategies: Insights into the Underlying Reaction Mechanisms," *Current Opinion in Chemical Engineering* 42 (2023): 100956, https://doi.org/10.1016/j.coche.2023.100956.

50. B. D. Etz and M. K. Shukla, "Per- and Polyfluoroalkyl Substances Chemical Degradation Strategies: Insights into the Underlying Reaction Mechanisms," *Current Opinion in Chemical Engineering* 42 (2023): 100956, https://doi.org/10.1016/j.coche.2023.100956.

51. P. Srivatsav, B. S. Bhargav, V. Shanmugasundaram, J. Arun, K. P. Gopinath, and A. Bhatnagar, "Biochar as an Eco-Friendly and Economical Adsorbent for the Removal of Colorants (Dyes) From Aqueous Environment: A Review," *Water* 12 (2020): 3561, https://doi.org/10.3390/w12123561.

52. Y. Wang, L. Chen, Y. Zhu, et al., "Research Status, Trends, and Mechanisms of Biochar Adsorption for Wastewater Treatment: A Scientometric Review," *Environmental Sciences Europe* 36, no. 1 (2024): 25, https://doi.org/10.1186/s12302-024-00859-z.

53. S. Kundu, S. Patel, P. Halder, et al., "Removal of PFASs From Biosolids Using a Semi-Pilot Scale Pyrolysis Reactor and the Application of Biosolids Derived Biochar for the Removal of PFASs From Contaminated Water," *Environmental Sciences* 7, no. 3 (2021): 638–649, https://doi.org/10.1039/d0ew00763c.

54. P. R. Yaashikaa, P. S. Kumar, S. Varjani, and A. Saravanan, "A Critical Review on the Biochar Production Techniques, Characterization, Stability and Applications for Circular Bioeconomy," *Biotechnology Reports* 28 (2020): e00570, https://doi.org/10.1016/j.btre.2020.e00570.

55. A. V. Bridgwater, "Review of Fast Pyrolysis of Biomass and Product Upgrading," *Biomass and Bioenergy* 38 (2012): 68–94, https://doi.org/10.1016/j.biombioe.2011.01.048.

56. W. C. Ng, S. You, R. Ling, K. Y.-H. Gin, Y. Dai, and C.-H. Wang, "Co-gasification of Woody Biomass and Chicken Manure: Syngas Production, Biochar Reutilization, and Cost-Benefit Analysis," *Energy* 139 (2017): 732–742, https://doi.org/10.1016/j.energy.2017.07.165.

57. P. R. Yaashikaa, P. S. Kumar, S. Varjani, and A. Saravanan, "A Critical Review on the Biochar Production Techniques, Characterization, Stability and Applications for Circular Bioeconomy," *Biotechnology Reports* 28 (2020): e00570, https://doi.org/10.1016/j.btre.2020.e00570.

58. V. Hansen, D. Müller-Stöver, J. Ahrenfeldt, J. K. Holm, U. B. Henriksen, and H. Hauggaard-Nielsen, "Gasification Biochar as a Valuable By-Product for Carbon Sequestration and Soil Amendment," *Biomass and Bioenergy* 72 (2015): 300–308, https://doi.org/10.1016/j.biombioe.2014.10.013.

59. V. Rajput, I. Saini, S. Parmar, et al., "Biochar Production Methods and Their Transformative Potential for Environmental Remediation," *Discover Applied Sciences* 6, no. 8 (2024): 408, https://doi.org/10.1007/s42452-024-06125-4.

60. P. Kumar, R. R. Singhania, Y. Sumathi, et al., *Clean Technologies and Environmental Policy* (2024).

61. S. Patel, M. Hedayati Marzbali, I. G. Hakeem, et al., "Production of H2 and CNM From Biogas Decomposition Using Biosolids-Derived Biochar and the Application of the CNM-Coated Biochar for PFAS Adsorption," *Waste Management* 159 (2023): 146–153, https://doi.org/10.1016/j.wasman.2023.01.037.

62. L. Zeng, J. Ma, J. Yang, J. Yang, X. Zeng, and Y. Zhou, "Ball Milling Nano-Sized Biochar: Bibliometrics, Preparation, and Environmental Application," *Environmental Science and Pollution Research* 31, no. 40 (2024): 52724–52739, https://doi.org/10.1007/s11356-024-34777-7.

63. J. M. Steigerwald and J. R. Ray, "Adsorption Behavior of Perfluorooctanesulfonate (PFOS) onto Activated Spent Coffee Grounds Biochar in Synthetic Wastewater Effluent," *Journal of Hazardous Materials Letters* 2 (2021): 100025, https://doi.org/10.1016/j.hazl.2021.100025.

64. P. M. Rodrigo, C. Navarathna, M. T. H. Pham, et al., "Batch and Fixed Bed Sorption of Low to Moderate Concentrations of Aqueous Per-

and Poly-Fluoroalkyl Substances (PFAS) on Douglas Fir Biochar and its Fe3O4 Hybrids," *Chemosphere* 308 (2022): 136155, https://doi.org/10.1016/j.chemosphere.2022.136155.

65. J. M. Steigerwald, S. Peng, and J. R. Ray, "Novel Perfluorooctanesulfonate-Imprinted Polymer Immobilized on Spent Coffee Grounds Biochar for Selective Removal of Perfluoroalkyl Acids in Synthetic Wastewater," *ACS ES&T Engineering* 3, no. 4 (2023): 520–532, https://doi.org/10.1021/acsestengg.2c00336.

66. A. Dąbrowski, "Adsorption — From Theory to Practice," *Advances in Colloid and Interface Science* 93, no. 1-3 (2001): 135–224, https://doi.org/10.1016/s0001-8686(00)00082-8.

67. J.-M. Herrmann, "Heterogeneous Photocatalysis: Fundamentals and Applications to the Removal of Various Types of Aqueous Pollutants," *Catalysis Today* 53, no. 1 (1999): 115–129, https://doi.org/10.1016/s0920-5861(99)00107-8.

68. S. Krebsbach, J. He, S. Adhikari, et al., "Mechanistic Understanding of Perfluorooctane Sulfonate (PFOS) Sorption by Biochars," *Chemosphere* 330 (2023): 138661, https://doi.org/10.1016/j.chemosphere.2023.138661.

69. M. A. N. Shaikh, P. Sarkar, and T. Nawaz, "PFOA Remediation From Aqueous Media Using CTAB Impregnated Activated Carbon: A Closed-Loop Sustainable Study With Comprehensive Selectivity Analysis," *Journal of Water Process Engineering* 54 (2023): 103965, https://doi.org/10.1016/j.jwpe.2023.103965.

70. S. Sudan, A. Khajuria, and J. Kaushal *Materials Today Proceedings* (2023).

71. Y. Zhang, X. Tan, R. Lu, et al., "Enhanced Removal of Polyfluoroalkyl Substances by Simple Modified Biochar: Adsorption Performance and Theoretical Calculation," *ACS ES&T Water* 3 (2023): 817–826, https://doi.org/10.1021/acsestwater.2c00597.

72. S. P. Lenka, M. Kah, and L. P. Padhye, "A Review of the Occurrence, Transformation, and Removal of Poly- and Perfluoroalkyl Substances (PFAS) in Wastewater Treatment Plants," *Water Research* 199 (2021): 117187, https://doi.org/10.1016/j.watres.2021.117187.

73. B. Yan, G. Munoz, S. Sauvé, and J. Liu, "Molecular Mechanisms of Per- and Polyfluoroalkyl Substances on a Modified Clay: A Combined Experimental and Molecular Simulation Study," *Water Research* 184 (2020): 116166, https://doi.org/10.1016/j.watres.2020.116166.

74. M. Askeland, B. O. Clarke, S. A. Cheema, A. Mendez, G. Gasco, and J. Paz-Ferreiro, "Biochar Sorption of PFOS, PFOA, PFHxS and PFHxA in Two Soils With Contrasting Texture," *Chemosphere* 249 (2020): 126072, https://doi.org/10.1016/j.chemosphere.2020.126072.

75. M. Sörengård, E. Östblom, S. Köhler, and L. Ahrens, "Adsorption Behavior of Per- and Polyfluoralkyl Substances (PFASs) to 44 Inorganic and Organic Sorbents and Use of Dyes as Proxies for PFAS Sorption," *Journal of Environmental Chemical Engineering* 8, no. 3 (2020): 103744, https://doi.org/10.1016/j.jece.2020.103744.

76. A. Kumar, S. Sidharth, and B. Kandasubramanian, "A Review on Algal Biosorbents for Heavy Metal Remediation With Different Adsorption Isotherm Models," *Environmental Science and Pollution Research* 30, no. 14 (2023): 39474–39493, https://doi.org/10.1007/s11356-023-25710-5.

77. S. Azizian, "Kinetic Models of Sorption: A Theoretical Analysis," *Journal of Colloid and Interface Science* 276, no. 1 (2004): 47–52, https://doi.org/10.1016/j.jcis.2004.03.048.

78. J. López-Luna, L. E. Ramírez-Montes, S. Martinez-Vargas, et al., "Linear and Nonlinear Kinetic and Isotherm Adsorption Models for Arsenic Removal by Manganese Ferrite Nanoparticles," *SN Applied Sciences* 1, no. 8 (2019): 950, https://doi.org/10.1007/s42452-019-0977-3.

79. H. Qiu, L. Lv, B. Pan, Q. Zhang, W. Zhang, and Q. Zhang, "Critical Review in Adsorption Kinetic Models," *Journal of Zhejiang University - Science* 10, no. 5 (2009): 716–724, https://doi.org/10.1631/jzus.a0820524.

80. J. Wang and X. Guo, "Adsorption Isotherm Models: Classification, Physical Meaning, Application and Solving Method," *Chemosphere* 258 (2020): 127279, https://doi.org/10.1016/j.chemosphere.2020.127279.

81. N. Mayilswamy, A. Nighojkar, M. Edirisinghe, S. Sundaram, and B. Kandasubramanian, "Sludge-derived Biochar: Physicochemical Characteristics for Environmental Remediation," *Applied Physics Reviews* 10, no. 3 (2023), https://doi.org/10.1063/5.0137651.

82. M. Anand, S. A. Farooqui, R. Kumar, et al., "Kinetics, Thermodynamics and Mechanisms for Hydroprocessing of Renewable Oils," *Applied Catalysis A: General* 516 (2016): 144–152, https://doi.org/10.1016/j.apcata.2016.02.027.

83. K. M. Doke and E. M. Khan, "Adsorption Thermodynamics to Clean up Wastewater; Critical Review," *Reviews in Environmental Science and Biotechnology* 12, no. 1 (2013): 25–44, https://doi.org/10.1007/s11157-012-9273-z.

84. M. Lowe, R. Qin, and X. Mao, "A Review on Machine Learning, Artificial Intelligence, and Smart Technology in Water Treatment and Monitoring," *Water (Basel)* 14, no. 9 (2022): 1384, https://doi.org/10.3390/w14091384.

85. A. Nighojkar, K. Zimmermann, M. Ateia, et al., "Application of Neural Network in Metal Adsorption Using Biomaterials (BMs): A Review," *Environmental Sciences: Advances* 2, no. 1 (2023): 11–38, https://doi.org/10.1039/d2va00200k.

86. Y. B. A. C. Ian Goodfellow, "Deep Learning."

87. B. Yegnanarayana, "Artificial Neural Networks."

88. R. E. Uhrig, "Introduction to Artificial Neural Networks," in *Proceedings of IECON '95 - 21st Annual Conference on IEEE Industrial Electronics* (New York City, USA: Institute for Electrical and Electronics Engineers (IEEE), 2008).

89. H. Samet, "K-nearest Neighbor Finding Using MaxNearestDist," *IEEE Transactions on Pattern Analysis and Machine Intelligence* 30, no. 2 (2008): 243–252, https://doi.org/10.1109/tpami.2007.1182.

90. L. Jiang, Z. Cai, D. Wang, and S. Jiang, "Survey of Improving K-Nearest-Neighbor for Classification," in *Fourth International Conference on Fuzzy Systems and Knowledge Discovery (FSKD 2007)* (New York City, USA: Institute for Electrical and Electronics Engineers (IEEE), 2007).

91. M. S Gaya, L. A. Yusuf, M. Mustapha, et al., *Indonesian Journal of Electrical Engineering and Computer Science* 5 (2017): 666.

92. Y. Zhu, "Estimation of an N–L–N Hammerstein–Wiener Model," *Automatica* 38, no. 9 (2002): 1607–1614, https://doi.org/10.1016/s0005-1098(02)00062-6.

93. S. I. Abba, Q. B. Pham, A. G. Usman, et al., "Emerging Evolutionary Algorithm Integrated With Kernel Principal Component Analysis for Modeling the Performance of a Water Treatment Plant," *Journal of Water Process Engineering* 33 (2020): 101081, https://doi.org/10.1016/j.jwpe.2019.101081.

94. A. Wills, T. B. Schön, L. Ljung, and B. Ninness, "Identification of Hammerstein–Wiener Models," *Automatica* 49, no. 1 (2013): 70–81, https://doi.org/10.1016/j.automatica.2012.09.018.

95. W. Allafi, I. Zajic, K. Uddin, and K. J. Burnham, "Parameter Estimation of the Fractional-order Hammerstein–Wiener Model Using Simplified Refined Instrumental Variable Fractional-order Continuous Time," *IET Control Theory & Applications* 11, no. 15 (2017): 2591–2598, https://doi.org/10.1049/iet-cta.2017.0284.

96. N. Karimi, S. Kazem, D. Ahmadian, H. Adibi, and L. V. Ballestra, "On a Generalized Gaussian Radial Basis Function: Analysis and Applications," *Engineering Analysis with Boundary Elements* 112 (2020): 46–57, https://doi.org/10.1016/j.enganabound.2019.11.011.

97. M. J. D. Powell, "Approximation Theory and Methods."

98. K. Baddari, T. Aïfa, N. Djarfour, and J. Ferahtia, "Application of a Radial Basis Function Artificial Neural Network to Seismic Data Inversion," *Computers & Geosciences* 35, no. 12 (2009): 2338–2344, https://doi.org/10.1016/j.cageo.2009.03.006.

99. R. DiPietro and G. D. Hager, "Deep Learning: RNNs and LSTM," in *Handbook of Medical Image Computing and Computer Assisted Intervention* (Amsterdam, Netherlands: Academic Press, Elsevier, 2020), 503.

100. M. S. A. G. A. G. N. L. N. N. Hongce Zhang, "Verification of Recurrent Neural Networks for Cognitive Tasks via Reachability Analysis."

101. S. Hochreiter and J. Schmidhuber, "Long Short-Term Memory," *Neural Computation* 9, no. 8 (1997): 1735–1780, https://doi.org/10.1162/neco.1997.9.8.1735.

102. A. P. J. Kamilya Smagulova, "Deep Learning Classifiers With Memristive Networks," 2020, 14.

103. P. Kim, "MATLAB Deep Learning," 2017.

104. U. R. Acharya, S. L. Oh, Y. Hagiwara, et al., "A Deep Convolutional Neural Network Model to Classify Heartbeats," *Computers in Biology and Medicine* 89 (2017): 389–396, https://doi.org/10.1016/j.compbiomed.2017.08.022.

105. J. Gu, Z. Wang, J. Kuen, et al., "Recent Advances in Convolutional Neural Networks," *Pattern Recognition* 77 (2018): 354–377, https://doi.org/10.1016/j.patcog.2017.10.013.

106. V. Dumoulin, F. Visin, 2016.

107. Q.-Y. Zhu, A. K. Qin, P. N. Suganthan, and G.-B. Huang, "Evolutionary Extreme Learning Machine," *Pattern Recognition* 38, no. 10 (2005): 1759–1763, https://doi.org/10.1016/j.patcog.2005.03.028.

108. G.-B. Huang, Q.-Yu Zhu, and C.-K. Siew, "Extreme Learning Machine: A New Learning Scheme of Feedforward Neural Networks," in *2004 IEEE International Joint Conference on Neural Networks (IEEE Cat. No.04CH37541)* (New York City, USA: Institute for Electrical and Electronics Engineers (IEEE), 2004).

109. G.-B. Huang, Q.-Y. Zhu, and C.-K. Siew, "Extreme Learning Machine: Theory and Applications," *Neurocomputing* 70, no. 1-3 (2006): 489–501, https://doi.org/10.1016/j.neucom.2005.12.126.

110. K. Zhang, S. Zhong, and H. Zhang, "Predicting Aqueous Adsorption of Organic Compounds Onto Biochars, Carbon Nanotubes, Granular Activated Carbons, and Resins With Machine Learning," *Environmental Science & Technology* 54, no. 11 (2020): 7008–7018, https://doi.org/10.1021/acs.est.0c02526.

111. E. Karbassiyazdi, F. Fattahi, N. Yousefi, et al., "XGBoost Model as an Efficient Machine Learning Approach for PFAS Removal: Effects of Material Characteristics and Operation Conditions," *Environmental Research* 215 (2022): 114286, https://doi.org/10.1016/j.envres.2022.114286.

112. B. Saawarn, B. Mahanty, and S. Hait, "Adsorptive Removal of Perfluorooctanoic Acid From Aqueous Matrices Using Peanut Husk-Derived Magnetic Biochar: Statistical and Artificial Intelligence Approaches, Kinetics, Isotherm, and Thermodynamics," *Chemosphere* 360 (2024): 142397, https://doi.org/10.1016/j.chemosphere.2024.142397.